Near Term ICF Target Test Chambers

R.L. Engelstad, P.L. Cousseau, G.L. Kulcinski

March 1996

FPA-96-2

FUSION POWER ASSOCIATES

2 Professional Drive, Suite 248
Gaithersburg, Maryland 20879
(301) 258-0545

1500 Engineering Drive
Madison, Wisconsin 53706
(608) 263-2308

Near Term ICF Target Test Chambers

R. L. Engelstad, P. L. Cousseau, and G. L. Kulcinski

Fusion Power Associates
402 Gammon Place
Suite 280
Madison, WI 53719

March 1996

FPA-96-2

1. INTRODUCTION

1.1 General Perspectives

For over 15 years, scientists and engineers in the U.S. ICF program have studied test chambers designed to contain single target explosions with yields of up to 1000 MJ. For the most part, these chambers have been coupled to laser or light ion beam drivers. The University of Wisconsin (UW) Fusion Technology Institute (FTI) has been involved in 4 of the chamber designs since 1980 [1.1-1.43]. The mechanical design and dynamic response of these chambers have been analyzed over this period and several design codes have been developed.

The purpose of this brief report is to document the work performed in the past by the UW-FTI. As would be expected, the analyses performed in 1995 are much more advanced than those performed in 1980. However, no attempt has been made in this brief report to redo the earlier work with the most recent codes. The report is structured as follows: First, a short summary of the 4 studies performed (TDF, APEX, LMF and NIF) is given. Next, an explanation of the mechanical and dynamic response of each of the 4 chambers is given. This is followed by a discussion of the common features and problems encountered. No attempt has been made to give all the details of each design as these can be found in the references. Rather, the emphasis is placed on the key features of each design and a discussion of the common and uncommon attributes of each chamber. It should be noted that the NIF design is still evolving and is likely to do so over the next few years. The reader should recognize that feature and not be too surprised by radical change in the future.

1.2 References

(For UWFTI Reports on TDF)

[1.1] R.R. Peterson, K.J. Lee, and G.A. Moses, "Low Density Cavity Gas Fireball Dynamics in the Light Ion Beam Target Development Facility," UWFDM-442, October 1981 [Proc. of the 9th Symposium on Engr. Prob. of Fusion Research, Chicago, IL, October 26-29, 1981].

[1.2] R.R. Peterson, K.J. Lee, and G.A. Moses, "Fireball Propagation in Preformed Plasma Channels in the Light Ion Beam Driven Target Development Facility," UWFDM-455, January 1982.

[1.3] R.R. Peterson, G.A. Moses, and K.J. Lee, "Choice of First Wall Material in the Light Ion Beam Target Development Facility," UWFDM-456, February 1982.

[1.4] R.L. Engelstad and E.G. Lovell, "Analysis and Design of ICF Target Development Facility First Wall Reinforcing Structures," UWFDM-478, July 1982.

[1.5] E.G. Lovell and R.L. Engelstad, "Dynamic Stress Analysis of Light Ion Fusion Target Development Facility Reaction Chambers," UWFDM-510, May 1983 [Presented at the Fifth ANS Topical Meeting on the Technology of Fusion Energy, 26-28 April 1983, Knoxville, TN].

[1.6] K.J. O'Brien, G.A. Moses, and A.M. White, "Neutron Activation and Shielding of the Light Ion Fusion Target Development Facility," UWFDM-512, May 1983 [Presented at the Fifth ANS Topical Meeting on the Technology of Fusion Energy, 26-28 April 1983, Knoxville, TN; Nucl. Tech./Fusion 4, 883 (1983)].

[1.7] R.R. Peterson and G.A. Moses, "Target Explosion Generated Fireballs in the Nitrogen Filled Target Chamber of the Light Ion Fusion Target Development Facility," UWFDM-515, May 1983 [presented at the Fifth ANS Topical Meeting on the Technology of Fusion Energy, 26-28 April 1983, Knoxville, TN; Nucl. Tech./Fusion 4, 860 (1983)].

[1.8] G.A. Moses, R.R. Peterson, R.L. Engelstad, E.G. Lovell, G.L. Kulcinski, K.J. O'Brien, A.M. White, J.J. Watrous, and D.L. Cook, "Light Ion Fusion Target Development Facility Preconceptual Design," UWFDM-521, May 1983 [Presented at the Fifth ANS Topical Meeting on the Technology of Fusion Energy, 26-28 April 1983, Knoxville, TN; Nucl. Tech./Fusion 4, 961 (1983)].

[1.9] R.R. Peterson, E.G. Lovell, R.L. Engelstad, G.L. Kulcinski, G.A. Moses, and K.J. Lee, "First Wall Materials Selection for the Light Ion Fusion Target Development Facility," UWFDM-522, May 1983 [Presented at the Fifth ANS Topical Meeting on the Technology of Fusion Energy, 26-28 April 1983, Knoxville, TN; Nucl. Tech./Fusion 4, 872 (1983)].

[1.10] M. Uesaka and G.A. Moses, "Parametric Survey of Microfireball Calculations for the Light Ion Fusion Target Development Facility Design," UWFDM-533, August 1983.

[1.11] E.G. Lovell, R.L. Engelstad and G.A. Moses, "Hydrostatic Instability of Target Development Facility Reaction Chamber," UWFDM585, June 1984.

[1.12] G.A. Moses, R.R. Peterson, M.E. Sawan and E.G. Lovell, "Target Diagnostics Package for the Light Ion Beam Fusion Target Development Facility," UWFDM-593, September 1984.

[1.13] R.L. Engelstad, E.G. Lovell and G.A. Moses, "Fatigue Stress Analysis of the Sandia TDF Reaction Chamber," UWFDM-594, September 1984 [Fusion Technology 8, 1890 (1985)].

[1.14] B. Badger, R.L. Engelstad, D.L. Henderson, E.G. Lovell, C.W. Maynard, G.A. Moses, Z. Musicki, R.R. Peterson, I.N. Sviatoslavsky, and J.J. Watrous, "Light Ion

Beam Fusion Target Development Facility Studies - Final Report for the Period January 27, 1984 to September 30, 1984," UWFDM-610, December 1984.

[1.15] Robert R. Peterson, John J. Watrous and Gregory A. Moses, "Microfireball Propagation in Z-Discharge Plasma Channels in the Light Ion Fusion Target Development Facility," UWFDM-613, January 1985.

[1.16] R.L. Engelstad, E.G. Lovell and G.A. Moses, "Fatigue Strength Analysis of the Sandia Target Development Facility Reaction Chamber," UWFDM-618, February 1985 [Presented at the Sixth Topical Meeting on the Technology of Fusion Energy, San Francisco, CA, 3-7 March 1985; Fusion Technology 8, 1890-1894 (July 1985)].

[1.17] R.R. Peterson, G.A. Moses, R.L. Engelstad, D.L. Henderson, G.L. Kulcinski, E.G. Lovell, M.E. Sawan, I.N. Sviatoslavsky, J.J. Watrous, R.E. Olson, D.L. Cook, "Light Ion Fusion Target Development Facility Preliminary Design," UWFDM-627, February 1985 [Presented at the Sixth Topical Meeting on the Technology of Fusion Energy, San Francisco, CA, 3-7 March 1985; Fusion Technology 8, 1895-1900 (July 1985)].

[1.18] D.L. Henderson, R.R. Peterson, and G.A. Moses, "Radioactivity Induced in the First Wall of the Light Ion Fusion Target Development Facility," UWFDM-628, February 1985 [Presented at the Sixth Topical Meeting on the Technology of Fusion Energy, San Francisco, CA, 3-7 March 1985; Fusion Tech. 8, (July 1985)].

[1.19] D.L. Henderson, G.A. Moses and R.R. Peterson, "One-Dimensional Activation and Radiological Dose Calculations for the Light Ion Fusion Target Development Facility," UWFDM-636, October 1985.

[1.20] R.L. Engelstad and E.G. Lovell, "Dynamic Response of Target Development Facility Spherical Chambers," UWFDM-655, October 1985.

[1.21] R.L. Engelstad and E.G. Lovell, "Parametric Lifetime Analysis of Cylindrical Chambers for the Target Development Facility," UWFDM-656, October 1985.

[1.22] G.A. Moses, R.R. Peterson, R.L. Engelstad, D.L. Henderson, G.L. Kulcinski, E.G. Lovell, I.N. Sviatoslavsky, J.J. Watrous, R.E. Olson and D.L. Cook, "Preconceptual Design of the Light Ion Beam Fusion Target Development Facility," UWFDM-664, November 1985 [Presented at 11th Symposium on Fusion Engineering, November 18-22, 1985, Austin, TX].

[1.23] Robert R. Peterson, Gregory A. Moses, John J. Watrous, R.E. Olson, "Plasma Channels for Light Ion Beam Propagation in the Target Development Facility," UWFDM-666, November 1985 [Presented at 11th Symposium on Fusion Engineering, November 18-22, 1985, Austin, TX].

[1.24] T.J. Bartel, G.A. Moses and R.R. Peterson, "Microfireballs in Stratified Target Chamber Gases in the Light Ion Target Development Facility - Final Report for the Period September 9, 1983 to September 30, 1985," UWFDM-677, September 1985.

[1.25] Jim Herzog, "Computation of Chemical Equilibrium in a Constant Temperature and Pressure System," UWFDM-695, June 1986.

[1.26] D.L. Henderson, M.E. Sawan and G.A. Moses, "Radiological Dose Calculations for the Diode Region of the Light Ion Fusion Target Development Facility," UWFDM-707, October 1986.

[1.27] O. Yasar, M.E. Sawan, D.L. Henderson and G.A. Moses, "Radiological Dose Calculations for the Chamber and Diode Region of the Light Ion Fusion Target Development Facility," UWFDM-726, July 1987.

[1.28] R.R. Peterson, R.L. Engelstad, E.G. Lovell, G.A. Moses, "Target Chamber Designs for the Light Ion Fusion Target Development Facility," UWFDM-733, October 1987 [Presented at 12th Symposium on Fusion Engineering, Monterey, CA, 12-16 October 1987].

[1.29] O. Yasar, M.E. Sawan, D.L. Henderson, G.A. Moses, "Radiological Dose Calculations for the Chamber and Diode Region of the Light Ion Fusion Target Development Facility," UWFDM-734, October 1987 [Presented at 12th Symposium on Fusion Engineering, Monterey, CA, 12-16 October 1987].

(For UWFTI Reports on APEX)

[1.30 R.R. Peterson, R.L. Engelstad, G.A. Moses, E.G. Lovell, "Target Chamber Design Considerations for the APEX Light Ion Beam Fusion Facility," UWFDM-724, May 1987.

[1.31] G.A. Moses, R.L. Engelstad, E.G. Lovell, R.R. Peterson; R. Whitley, M. Connelly, B. Glasgow, A. Patel, R. Yamamoto (TRW Space and Technology Group); J. Callen, D. Engman, W. Kelber, E. Maltz (Facilities Systems Engineering Corp.), "Design Studies of the APEX Light Ion Fusion Experiment," UWFDM-735, October 1987 [Presented at 12th Symposium on Fusion Engineering, Monterey, CA, 12-16 October 1987].

(For UWFTI Reports on LMF)

[1.32] B. Badger, R.R. Peterson, R.L. Engelstad, M.E. Sawan, H. Khater, J.J. MacFarlane, G.A. Moses, E.G. Lovell, "Target Chamber Studies for a Light Ion Fusion Laboratory Microfusion Facility," UWFDM-768, August 1988.

[1.33] J.J. MacFarlane, R.R. Peterson and G.A. Moses, "Analysis of Physical Processes in ICF Target Chambers: Application to the Laboratory Microfusion Facility," UWFDM-776, October 1988 [Presented at the 8th Topical Meeting on the Technology of Fusion Energy, 9-13 October 1988, Salt Lake City, Utah].

[1.34] Robert R. Peterson, "Computer Simulation of the Destruction of a Close-In Diagnostic for the Laboratory Microfusion Facility," UWFDM-798, August 1989.

[1.35] Robert R. Peterson, "Experiments to Simulate X-Ray Damage to the First Wall of the Inertial Confinement Fusion Laboratory Microfusion Facility," UWFDM-806, October 1989 [Presented at the 13th Symposium on Fusion Engineering, 2-6 October 1989, Knoxville TN].

[1.36] H.Y. Khater and M.E. Sawan, "Dose Rate Calculations for a Light Ion Beam Fusion Laboratory Microfusion Facility," UWFDM-809, October 1989 [Presented at the 13th Symposium on Fusion Engineering, 2-6 October 1989, Knoxville TN].

[1.37] Robert R. Peterson, "X-Ray Effects on First Surfaces in the Inertial Confinement Fusion Laboratory Microfusion Facility," UWFDM-818, December 1989.

[1.38] Robert R. Peterson, Roxann L. Engelstad, John W. Powers, H.Y. Khater, Mohammed E. Sawan, Edward G. Lovell, Gregory A. Moses, "An Overview of Target Chamber Design and Analysis for the Light Ion Beam Laboratory Microfusion Facility," (Annual Report to Sandia National Laboratories for Work Performed 10/1/88 - 9/31/89), UWFDM-819, December 1989.

[1.39 R.L. Engelstad, J.W. Powers and E.G. Lovell, "Mechanical Design of the LMF Target Chamber," UWFDM-828, October 1990 [Presented at the 9th Topical Meeting on the Technology of Fusion Energy, 7-11 October 1990, Oak Brook, IL].

[1.40 R.R. Peterson, "Pressure Loadings on the Walls of a Light Ion Laboratory Microfusion Facility Target Chamber," UWFDM-833, October 1990 [Presented at the 9th Topical Meeting on the Technology of Fusion Energy, 7-11 October 1990, Oak Brook, IL].

[1.41 R.R. Peterson, R.L. Engelstad, R.D. Griffin, H.Y. Khater, E.G. Lovell, J.J. MacFarlane, G.A. Moses, J.W. Powers, S.C. Rutledge, M.E. Sawan, P. Wang, O. Yasar, "Target Chamber Issues for the Sandia National Laboratories Laboratory Microfusion Facility - Final Report for the Period 10/1/88 through 12/31/90," UWFDM-854, April 1991.

(For UWFTI Reports on NIF)

[1.42 R.R. Peterson, G.A. Moses, J.J. MacFarlane, P. Wang, "X-Ray and Debris Ion Spectra Emanating from NIF Targets," UWFDM-949, May 1994 [Prepared for the Eleventh Topical Meeting on the Technology of Fusion Energy, June 19-23, 1994, New Orleans, LA].

[1.43] R.R. Peterson, J.J. MacFarlane, P. Wang, "Response of the National Ignition Facility Target Chamber Walls to the Microexplosion of a Fusion Target," UWFDM-952, May 1994 [Prepared for the Eleventh Topical Meeting on the Technology of Fusion Energy, June 19-23, 1994, New Orleans, LA].

2. SUMMARY OF PAST U.S. ICF TARGET CHAMBERS

2.1 Target Development Facility (TDF)

The Target Development Facility (TDF) was a proposed light ion research facility of Sandia National Laboratories (SNL) to follow the Particle Beam Fusion Accelerator (PBFA-II). From 1980 to 1988, the University of Wisconsin - Madison (UW) was involved with the design of the TDF target chamber, intended to be the first chamber designed to withstand the environment created by high yield targets. The facility was expected to test 15,000 high yield shots (200 MJ) over a five year period at the average rate of 10 shots per day. Critical issues in the preconceptual design phase were addressed by the UW. They included: (a) the structural design of the target chamber to meet the fatigue lifetime criteria, (b) the design of the first surface to withstand the thermal loading of the target generated microfireball, (c) neutron activation of the target chamber, (d) the creation of plasma channels to efficiently transport the ion beams and (e) the design of a high power pulse driver and reusable diodes. Details of the structural design of the target chamber, including the chamber environment, are summarized in Section 3 of this report.

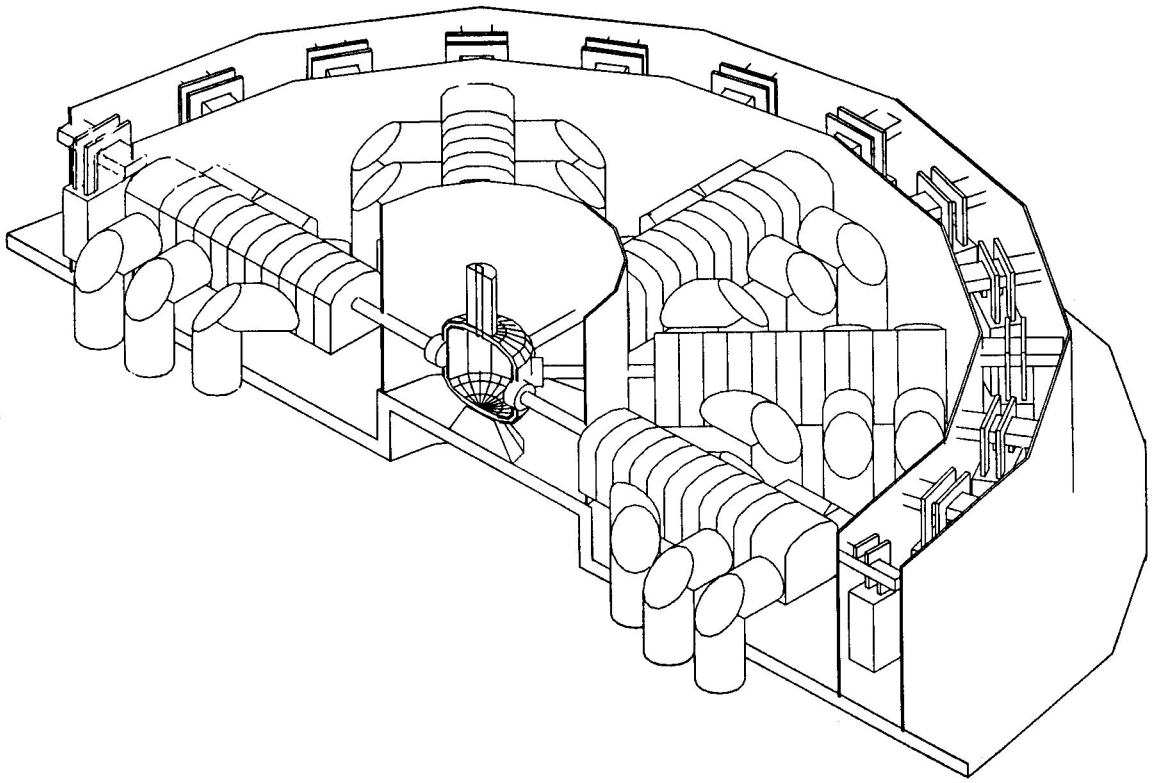

Fig. 2.1. Schematic of the Target Development Facility (TDF).

2.2 APEX Light Ion Beam Fusion Facility (APEX)

The Particle Beam Fusion Accelerator II (PBFA-II) at Sandia National Laboratories was designed to achieve significant thermonuclear burn in a DT fusion target, but not high gain. The target performance was originally thought to be limited by the pulse shaping capabilities of the diode-target configuration. In PBFA-II, lithium ions were ballistically focused from a 15 cm radius barrel-shaped diode surrounding the target at the center of the machine. For high gain, the pulse shape had to be reconfigured. This was the major purpose of the APEX upgrade project. Improvements in the pulse shaping came through voltage ramping of the ions in an extraction diode and injection into a z-pinch plasma channel with the target at the other end of the channel. With this new configuration, time-of-flight compression of the beam could generate the finely tuned temporal power profile that high gain targets required. The inclusion of the long plasma channel for APEX necessitated the modification of the basement of the PBFA-II facility. The target location was moved from the center of the PBFA-II chamber to the end of the new plasma channel in the basement. Here, the ion beam would enter a target chamber from the top, as shown in Fig. 2.2. Investigations on this research facility were conducted by Sandia National Laboratory, the Naval Research Laboratory, TRW and the University of Wisconsin - Madison during 1986 and 1987.

In summary, the APEX upgrade included: modification of the pulsed power, replacement of the barrel diode with an extraction diode, the addition of a z-pinch plasma channel and the design of a shielded target chamber. The design and analysis of the target chamber was the task assigned to the University of Wisconsin. The chamber was required to contain a 100 MJ target explosion with a total of 30 shots lifetime. Since the radioactivity induced following a single shot posed a severe problem, it was proposed to design a "throw away" chamber that was small enough to be remotely removed after each target explosion. Issues driving the chamber design involved the determination of the smallest chamber to contain the blast loading. In addition, vaporization and subsequent recondensation of the wall material complicated the analysis. Details of the chamber mechanical modeling and dynamic response are presented in Section 4 of this report.

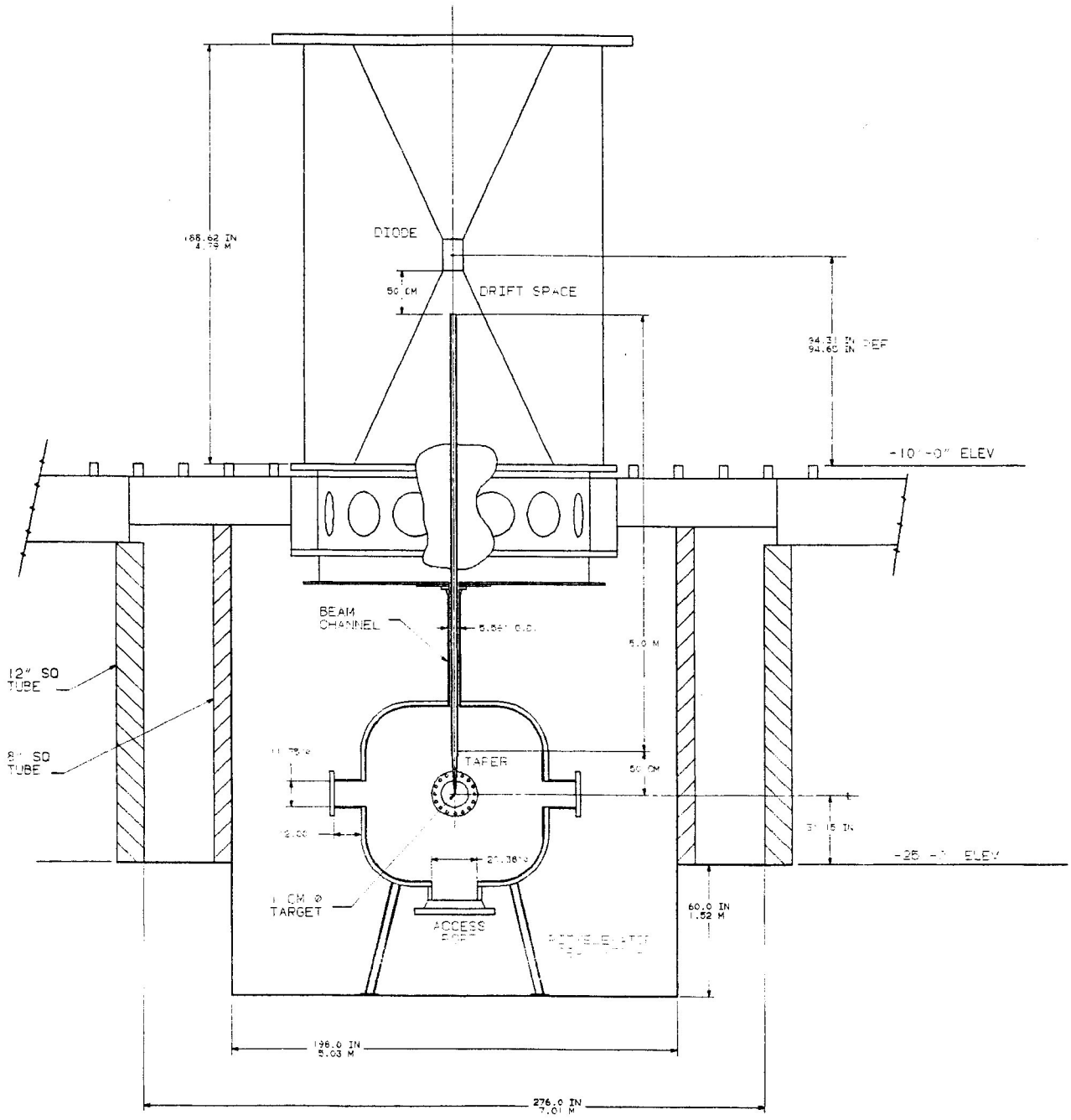

Fig. 2.2. Modification of PBFA-II to accommodate the APEX light ion fusion experiment.

2.3 Laboratory Microfusion Facility (LMF)

During the period between 1988 and 1991, the University of Wisconsin - Madison in conjunction with Sandia National Laboratories conducted research on a light ion beam Laboratory Microfusion Facility (LMF) shown in Fig. 2.3. Applications of the facility included the development of high gain, hield yield ICF targets. The efforts at Wisconsin included the mechanical analysis of critical aspects of the target chamber to identify the size of the structure, to compare the response of structrual materials and to establish basic design characteristics. The LMF target chamber had to meet the requirements imposed by the ion beam propagation and survive severe target blast loadings. Yields from 10 MJ to 1000 MJ were considered for a projected lifetime up to 15,000 shots. The chamber was to be subjected to repeated loadings that included intense x-ray vaporization of the first wall surface, resulting in large amplitude pressure waves. A carbon/carbon composite thermal liner was proposed to attenuate the radial shock waves and protect the structural first wall. Details of the chamber parameters, mechanical analysis and structural response are given in Section 5 of this report.

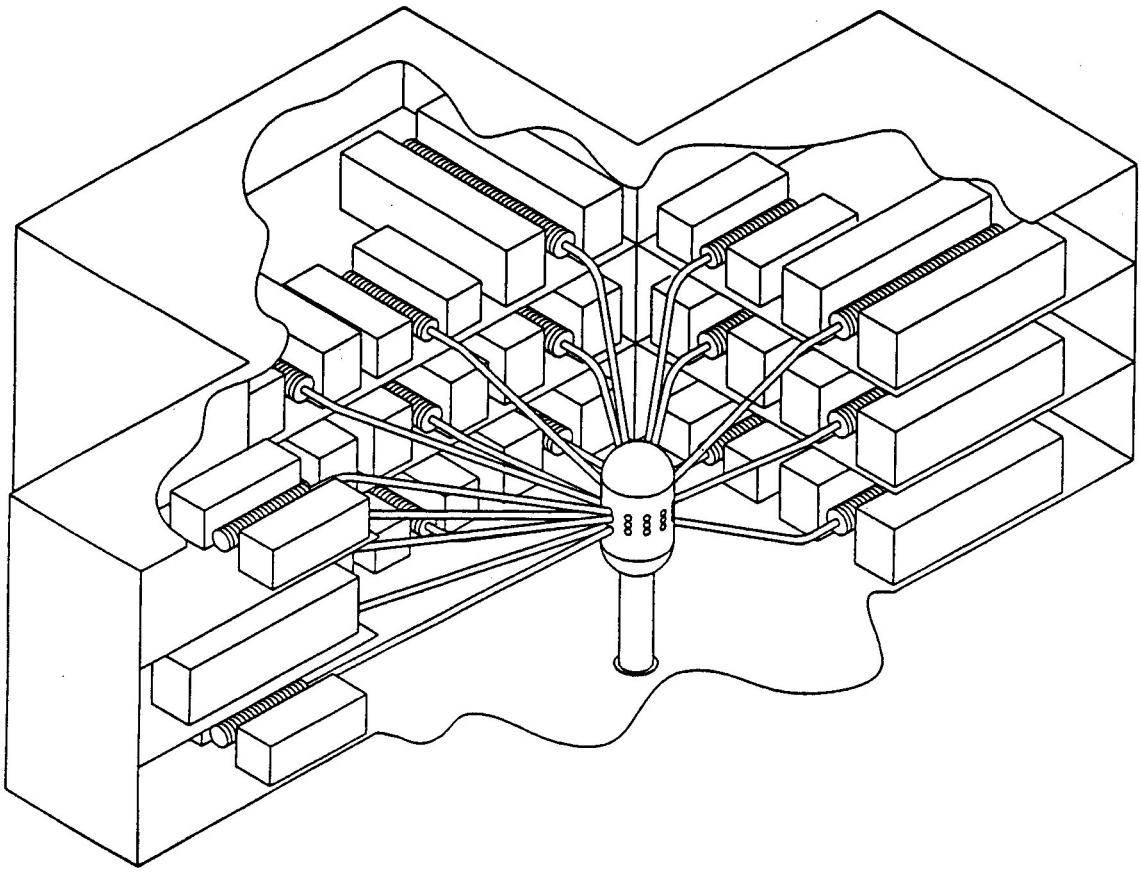

Fig. 2.3. Schematic of the Laboratory Microfusion Facility (LMF).

2.4 National Ignition Facility (NIF)

In January 1993, the Secretary of Energy Hazel O'Leary acknowledged the need for the National Ignition Facility (NIF) and authorized the three Department of Energy (DOE) national laboratories, Lawrence Livermore National Laboratory (LLNL), Los Alamos National Laboratory (LANL), Sandia National Laboratory (SNL), and the University of Rochester's Laboratory for Laser Energetics to produce a conceptual design report (CDR). In April 1994, the 7000 page report was finished and by October 1994, the Secretary approved NIF's continuation. This decision initiated the preliminary design, cost and schedule validation, safety analysis and a two year Environmental Impact Statement. LLNL was also specified as the preferred site for NIF. In August 1995, Ralph M. Parsons Company was selected as the architect engineer for the primary NIF facility, the Laser and Target Area Building. Albert C. Martin and Associates was chosen as the architect engineer for the NIF Optics Assembly Building. In January 1996, Sverdrup Facilities, Inc., was named as the NIF construction manager. The 1996 fiscal budget for NIF is $61 million, $23.6 million for operating funds which includes advanced conceptual design studies and $37.4 million in construction funds. The construction of NIF is planned from 1996 through 2002 at a cost of $1074 million; after completion it will cost $60 million per year to operate.

When finished, the NIF will be housed in a football stadium sized facility (see Fig. 2.4). It will focus 192 laser beams onto a target of fusion fuel inside a spherical chamber 10 m in diameter. The information obtained from NIF will help researchers evaluate inertial fusion as a new energy source. Section 6.1 of this report describes the conceptual design for NIF, detailing the geometry, loadings and support structure for the main target chamber. Sections 6.2-6.4 present the geometry and dynamics response for a proposed "minichamber" that would fit inside the main target chamber to protect the it from target shrapnel.

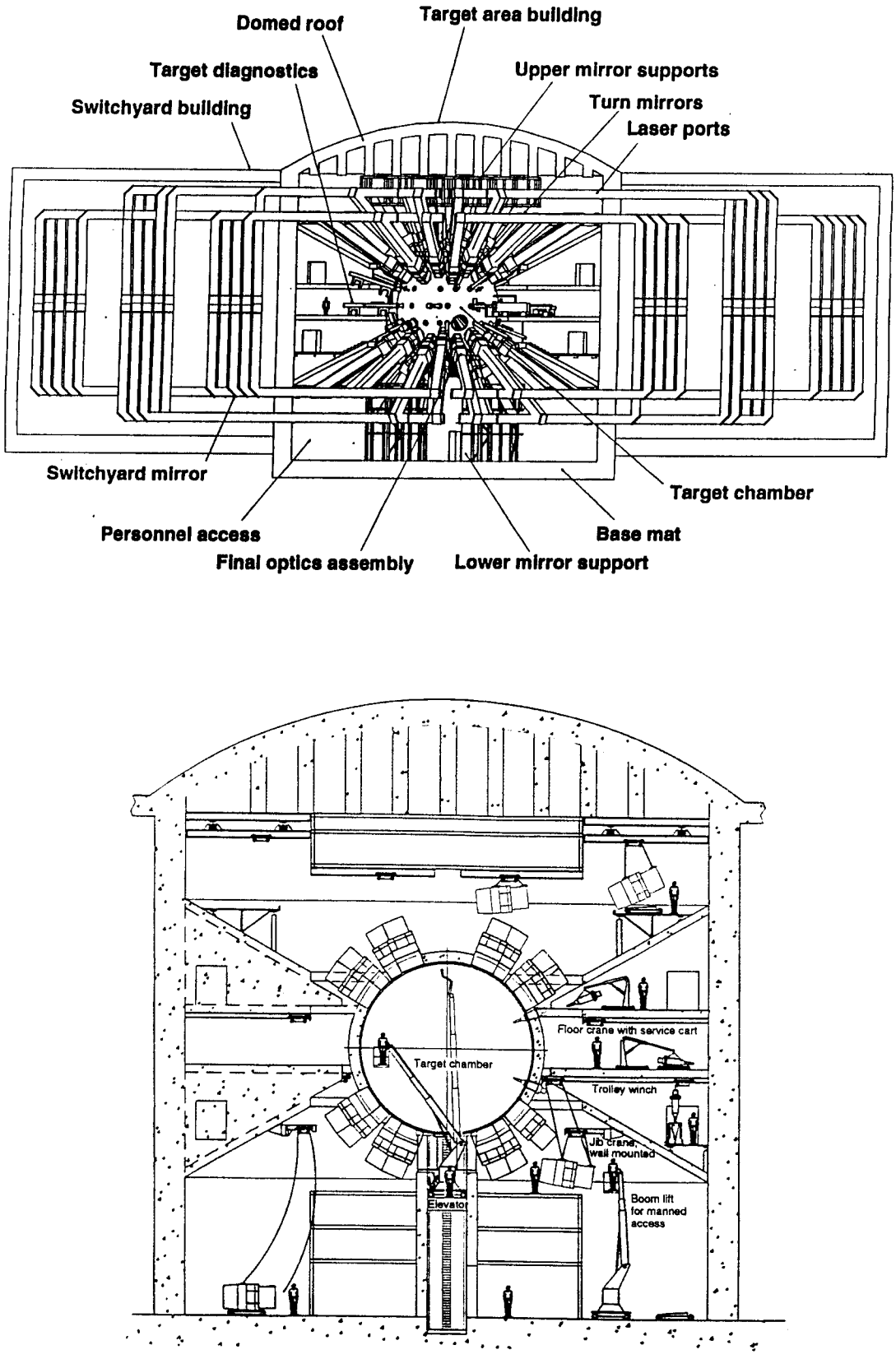

Fig. 2.4. Schematic of the National Ignition Facility (NIF) and target area. (J. Lindl, Phy. of Plasmas, Vol. 2, No. 11, pp. 3933, 1995.)

3. TARGET DEVELOPMENT FACILITY (TDF)

3.1 TDF Target Chamber Parameters and Conditions

One of the primary objectives of the TDF facility was to design a target chamber to withstand the environment created by high yield targets. The target yield for the base case was 200 MJ with a projected total of 15,000 shots over a five year period. The beams consisted of lithium atoms with energies between 25 MeV and 35 MeV and were propagated from ion diodes to the target through a target chamber gas in plasma channels. The energy released in the target explosion was about 72% in neutrons and 28% in x-rays and debris ions. The target x-rays and ions deposit their energy in the target chamber gas in a manner that generates a blast wave that mechanically and thermally loads the wall of the target chamber. Radioactivity induced in the target chamber structure also limited access to the chamber and required shielding of the chamber itself. In addition, diagnostics of the ion beams and the target were required and had to survive in the chamber environment.

Two target chamber designs were pursued, each facing the critical issues differently. The larger chamber design, shown in Fig. 3.1, attempted to minimize the induced radioactivity in the chamber structure with the use of a graphite moderator. The chamber was cylindrical in shape with a radius of 3.0 m, height of 6.0 m and included a graphite neutron moderator 0.5 m in thickness. Figure 3.2 shows the structure in detail.

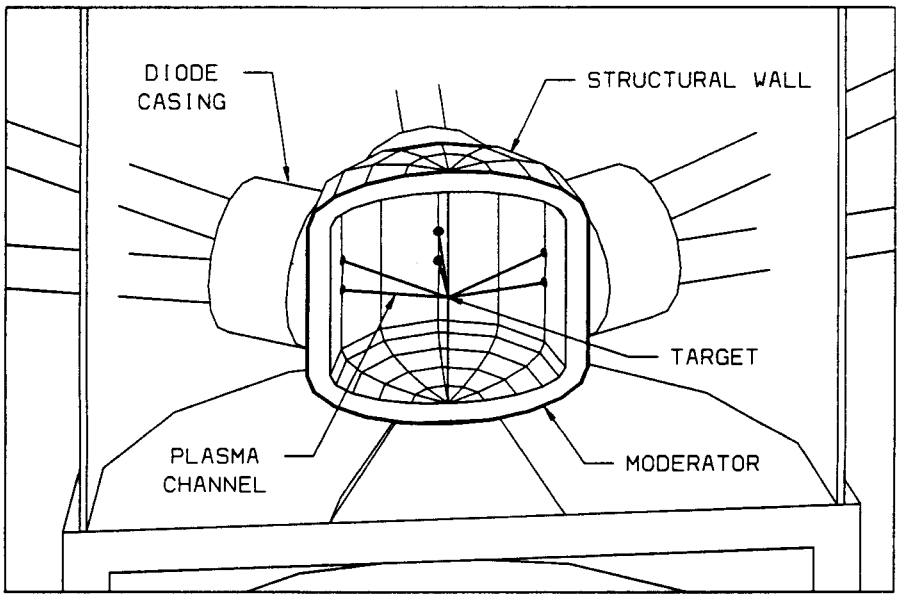

Fig. 3.1. TDF chamber design with graphite neutron moderator (3.0 m radius).

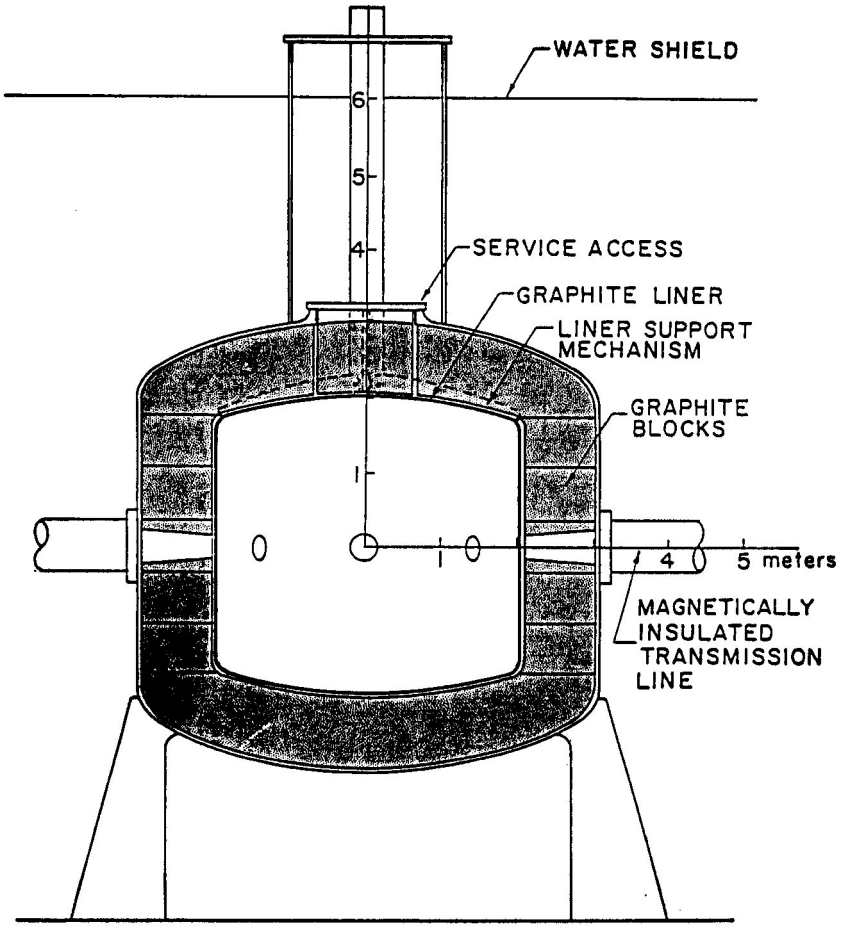

Fig. 3.2. Schematic of the TDF chamber design for the 3.0 m radius cylindrical structure.

The second chamber design was much smaller, i.e., a sphere 1.0 m in radius with only a thin liner of graphite (see Fig. 3.3). In this design, ion beams and radiation for diagnostics propagated through much less target chamber gas than in the first design.

The shell structure for both chambers had to accommodate 8 beam ports, although the actual diameter of the ports was relatively small. Therefore, the mechanical analysis assumed that adequate reinforcing could be used to eliminate any stress concentrations and unperforated shells were used to simulate the dynamic response. A listing of the mechanical parameters for both chambers is given in Table 3.1.

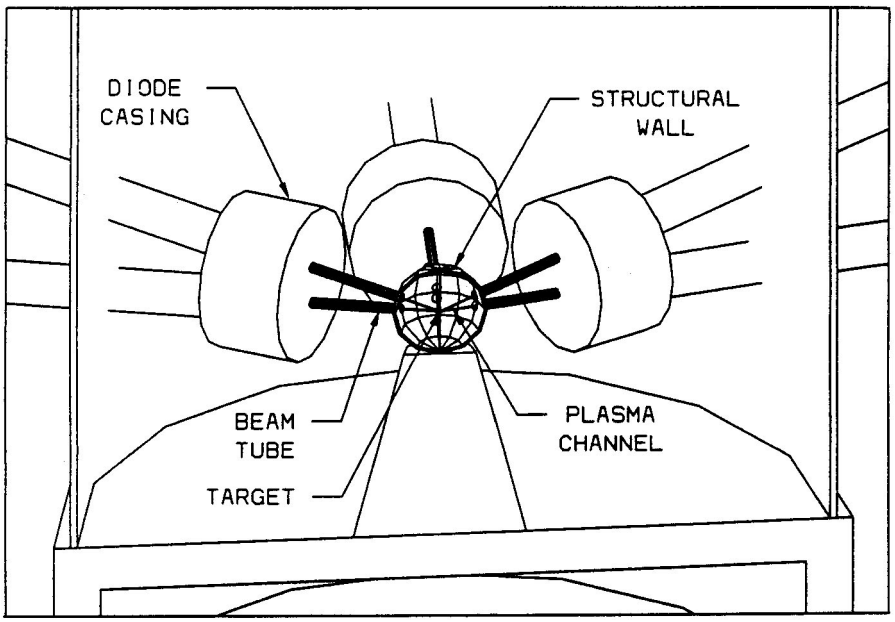

Fig. 3.3. TDF chamber design without the neutron moderator (1.0 m radius).

Table 3.1. Mechanical Parameters for the TDF Chambers.

Geometry	Cylindrical Shell	Spherical Shell
Radius	3.0 m	1.0 m
Cylindrical Wall Height	6.0 m	----
Number of Beam Ports	8	8
Port Diameters	10 cm	----
Fill Gas	14 torr Nitrogen	14 torr Nitrogen
Thermal Liner Thickness	50 cm	1 cm
Thermal Liner Material	Graphite	Graphite
Structural Materials	Al 6061-T6, or 2.25 Cr - 1 Mo Steel	Al 6061-T6, or 2.25 Cr - 1 Mo Steel

3.2 Hydrodynamics

As previously noted, the TDF chamber was to be designed to withstand a total of 15,000 shots over 5 years, giving an average shot rate of 10 per day. The typical target explosion would contain a total of 200 MJ with 14 torr of nitrogen gas in the chamber. Figure 3.4 shows the resulting pressure history on the first wall (for both chamber sizes) as calculated by the Lagrangian hydrodynamics code CONRAD [3.1]. For the 3.0 m radius chamber, the pressure falls to insignificant values from a 1.0 MPa maximum in about 0.3 ms. On the other hand, the 1.0 m radius chamber pressure remains high for a much longer time. This occurs because the energy deposited per unit mass in the gas is much higher in the smaller chamber. These calculations were thought to be conservative because the energy lost by the blast waves due to radiation was underestimated.

It should be noted that the loading on the 3.0 m chamber was impulsive in nature corresponding to 100 Pa-s for the 200 MJ case. In addition, the residual overpressure essentially dropped to zero. However, for the smaller chamber, the wall pressure remained significant for a much longer time (relatively speaking). Therefore, it could no longer be assumed that the pressure pulse duration was short compared to the vibrational period of the wall. Consequently, this loading was treated as a forced vibration.

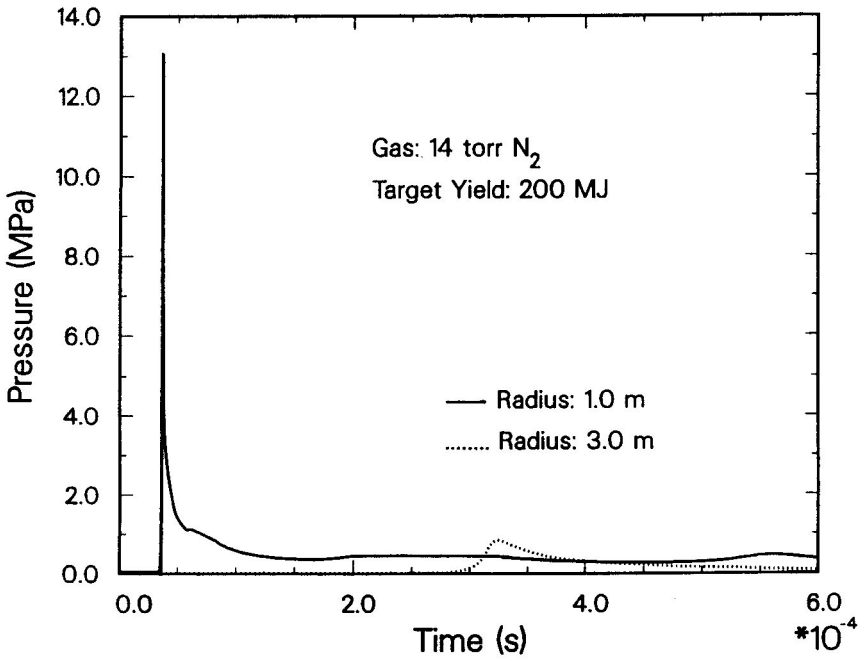

Fig. 3.4. Calculated blast overpressures on the first surface of the TDF chamber.

3.3 Mechanical Response

The mechanical and thermal loading of the TDF chambers were decoupled, assuming that the thermal liner would sustain the temperature loading. On the other hand, the graphite liner was considered to be a nonstructural assembly. Consequently, the chamber shell structure needed to withstand the full impact of the blast wave. The mechanical analyses presented here are based on the 200 MJ case presented in Section 3.2. In addition, two materials were considered for the target chamber, i.e., welded 6061-T6 aluminum and 2.25 Cr - 1 Mo ferritic steel.

For the cylindrical chamber, the maximum flexural stress occurs at the ends of the cylinder where it is assumed to be rigidly fixed, or clamped. However, the stress distribution is characterized by a rather steep axial gradient near the ends and can be controlled by a localized increase in thickness at this location. In the greater percentage of the shell which excludes the ends, the dominant stress is circumferential. The design thickness is based upon this value which is more uniformly distributed and also of smaller amplitude. Figure 3.5 shows the calculated circumferential stress history for an impulsive pressure of 100 Pa-s and a wall thickness of 5 cm. (The stresses for the two materials are virtually the same due to material property ratios, although the strains in the aluminum are approximately three times as high in the steel.) The analysis calculates the motion of the wall by summing over the linear vibrational modes the shell. The peak stress of 15 MPa corresponds to a doubled strain of 7.8×10^{-4} in aluminum, which is less than the endurance limit of 8.3×10^{-4}. The dynamic response is even more conservative in the steel. Therefore, the wall will survive more than the required 15,000 shots when either material is used.

In the smaller chamber, the governing equations of motion for a spherical shell are numerically integrated using the forced excitation given by the blast loading. The corresponding stress history is shown in Fig. 3.6, again for either material. The maximum stress and doubled strain range are 12 MPa and 3.2×10^{-4}, respectively, for aluminum. With the strain range below the endurance limit for both materials, the spherical chamber should also withstand 15,000 shots.

Further details on the design and analysis of the TDF target chamber can be found in References [3.2] to [3.4].

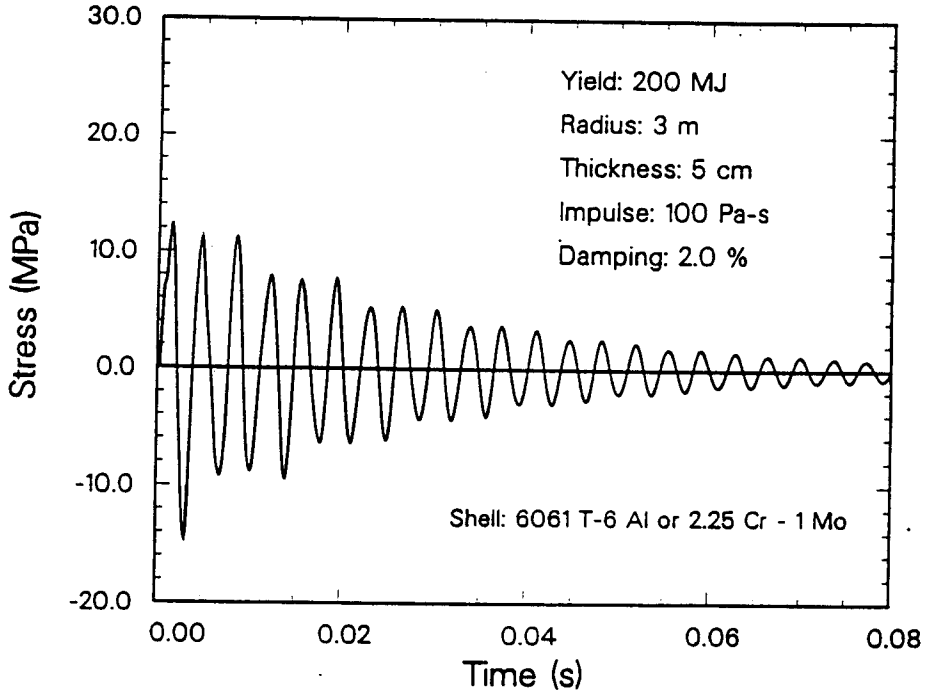

Fig. 3.5. Mechanical stresses in the TDF cylindrical chamber (3.0 m radius).

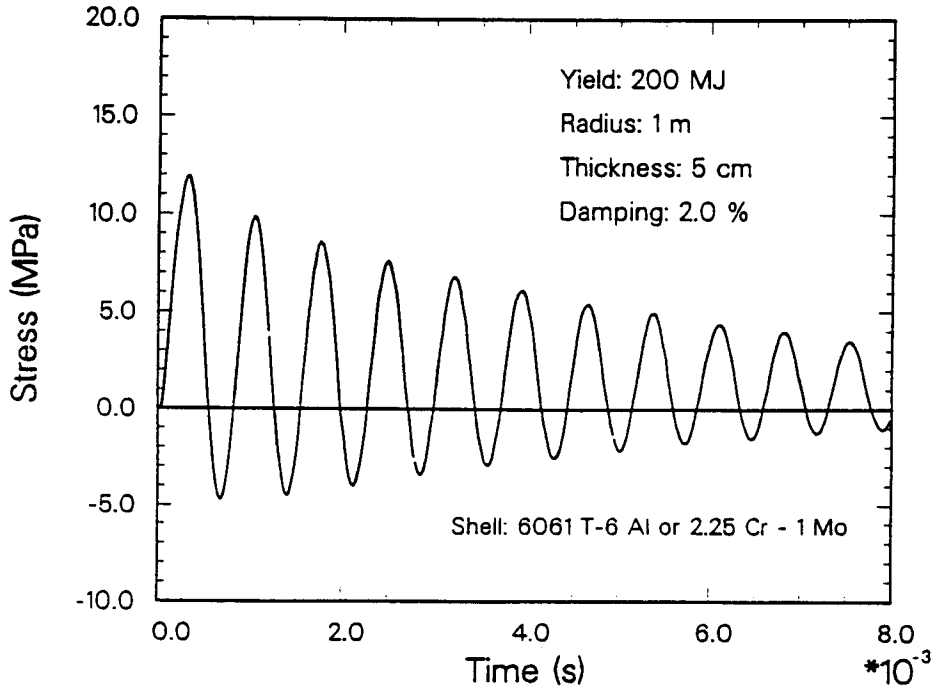

Fig. 3.6. Mechanical stresses in the TDF spherical chamber (1.0 m radius).

3.4 References

[3.1] R. R. Peterson, "CONRAD - A Combined Hydrodynamics-Vaporization/ Condensation Computer Code," UWFDM-670, University of Wisconsin Fusion Technology Institute Report, 1986.

[3.2] R. Engelstad and E. Lovell, "Lifetime Analysis of the TDF Reaction Chamber," UWFDM-665, University of Wisconsin Fusion Technology Institute Report, 1985.

[3.3] B. Badger et al., "Light Ion Beam Fusion Target Development Facility Studies: Progress Report for the Period 1 October 1985 to 31 October 1986," UWFDM-713, University of Wisconsin Fusion Technology Institute Report, 1986.

[3.4] B. Badger et al., "Light Ion Beam Fusion Target Development Facility Studies: Progress Report for the Period 1 November 1986 to 31 October 1987," UWFDM-752, University of Wisconsin Fusion Technology Institute Report, 1988.

4. APEX LIGHT ION FUSION FACILITY (APEX)

4.1 APEX Target Chamber Parameters and Conditions

The APEX project was intended to be the design of an experimental facility that could be constructed in the basement of the PBFA-II light ion fusion accelerator at Sandia National Laboratories. Specifically, the purpose of the APEX upgrade project was to allow pulse shaping for driving high gain ICF targets and containing the subsequent implosion and resulting radioactive debris. An unusual feature of the target chamber was that it was to be removed after a single shot so that the major source of induced radiation in the experimental facitlity was eliminated. For this reason, along with the fact that the chamber with shielding had to fit in the basement of PBFA-II, smaller chambers were preferred. Figure 4.1 shows a schematic of the target chamber with a radius of 1.0 m, although a smaller chamber with a 0.5 m radius was also considered. It was assumed that the outside of the chamber would be covered with 1.0 cm of boral to reduce activation and then submerged in a 4.0 m diameter tank of borated water. The inside of the chamber was to be protected with 1.0 cm thick carbon-carbon composite tiles to serve as a heat shield. For modeling purposes, the geometry of the chamber was assumed to be spherical with no perforations. The principal mechanical parameters of the system are listed in Table 4.1.

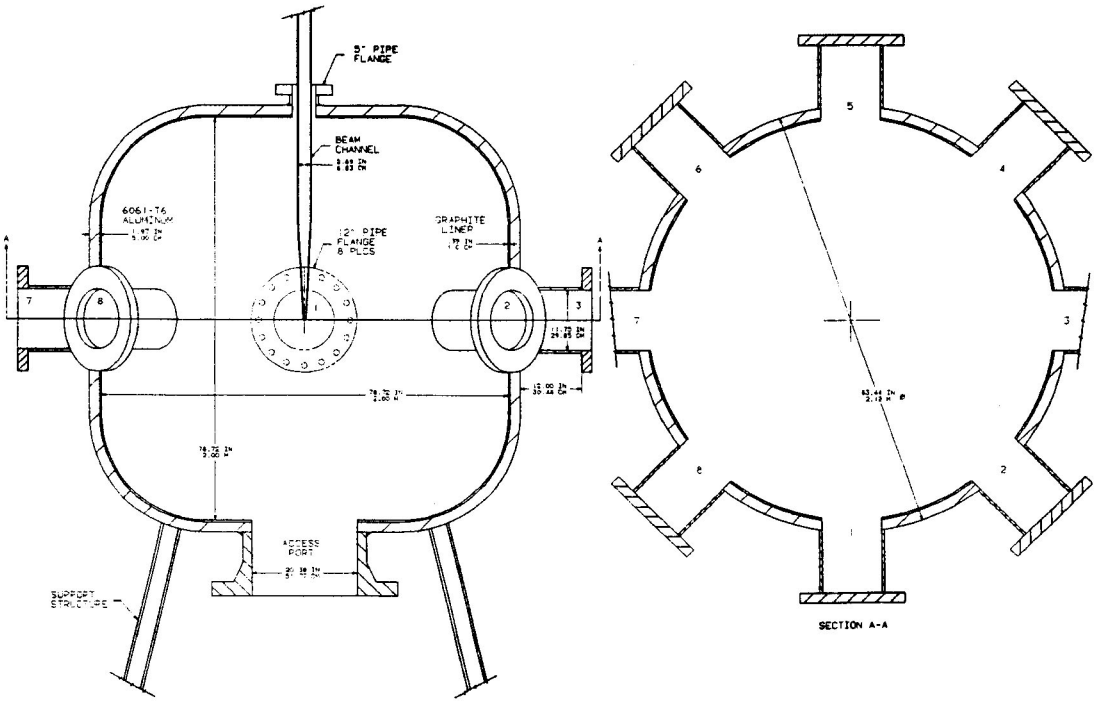

Fig. 4.1. Target chamber design for the APEX experiment.

Table 4.1. Mechanical Parameters for the APEX Chamber.

Geometry	Spherical
Radius	0.5 m or 1.0 m
Fill Gas	100 torr He
Thermal Liner Thickness	1.0 cm
Thermal Liner Material	Carbon/carbon composite
Structural Materials	Al 6061-T6, or 2.25 Cr - 1 Mo

4.2 Hydrodynamics

The design of the APEX target chamber was based upon a target yield of 100 MJ, and it was assumed that the cavity was initially filled with 100 torr of helium gas. The pressure loading on the chamber wall was thought of as stemming from three sources: the static pressure of the vaporized wall material that fills the target chamber, the impulse due to shocks in the gas that are caused by the target explosion and the recoil impulse from the vaporization of the wall material. Table 4.2 lists the pressure loadings on the first wall (for the two chamber sizes considered) as predicted by the radiation-hydrodynamics code CONRAD [4.1]. The actual pressure histories corresponding to the two cases are shown in Figs. 4.2 and 4.3.

Table 4.2. Pressure Loadings on the APEX Chamber.

Chamber Radius (m)	Impulsive Pressure (Pa-s)	Residual Pressure P_{static} (MPa)
0.5	75	5.47
1.0	120	1.6

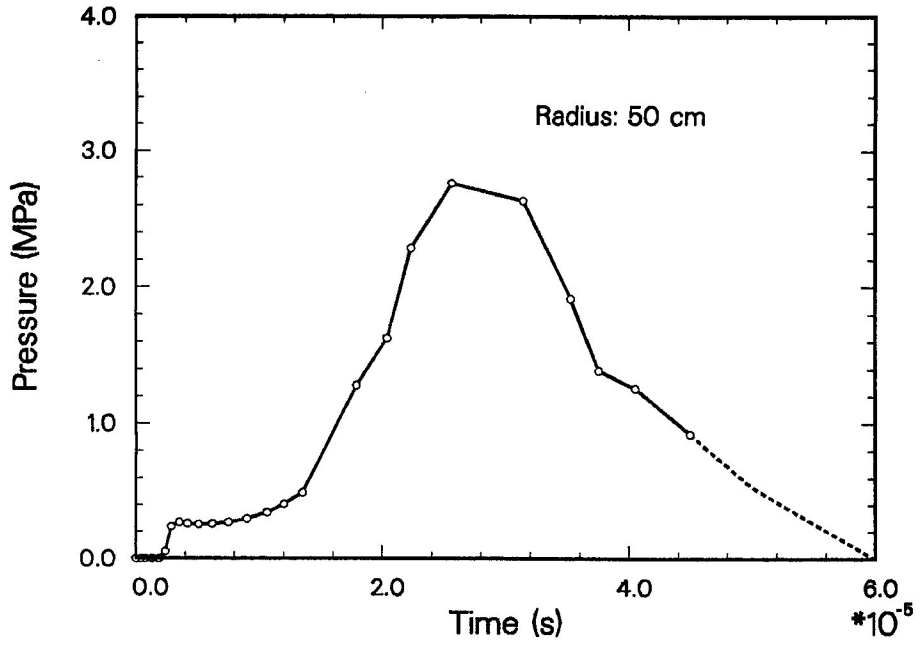

Fig. 4.2. Blast wave overpressure on APEX first wall (0.5 m radius).

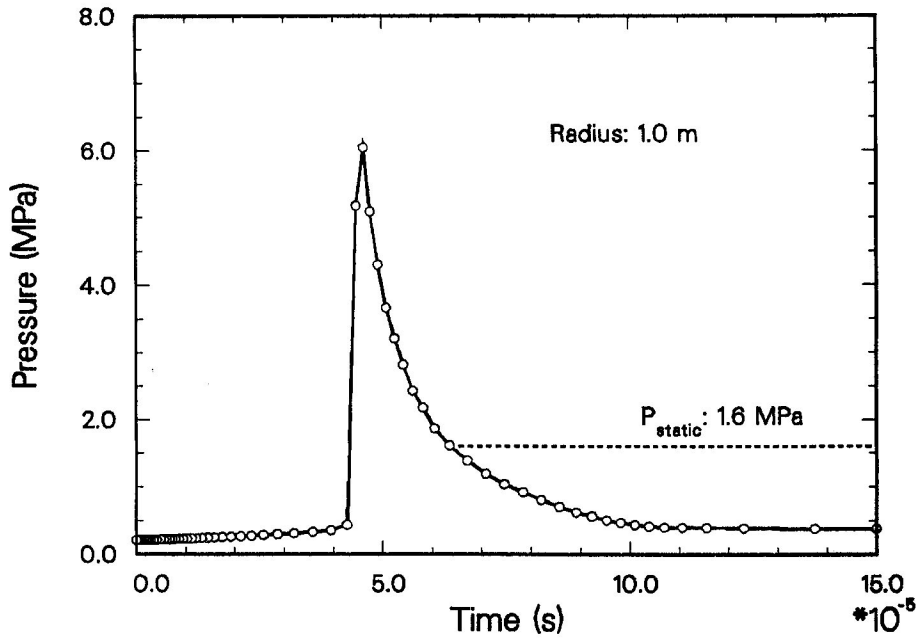

Fig. 4.3. Blast wave overpressure on APEX first wall (1.0 m radius).

4.3 Mechanical Response

The "throw-away" nature of the target chamber directs its design toward the smallest size consistent with an acceptable structural response to the target blast. Since each chamber experiences only one shot, the design criteria was to avoid rupturing. There were no fatigue considerations of importance. Two materials were investigated for the APEX chamber design, i.e., 2.25 Cr - 1 Mo and 6061-T6 aluminum. Table 4.3 lists the material property data on both used in all calculations [4.2].

Table 4.3. Static Properties of Chamber Materials.

	Unwelded Al 6061 - T6	Steel 2.25 Cr - 1 Mo
Yield Strength	270MPa	255 MPa
Ultimate Strength	305 MPa	504 MPa
Elastic Modulus	68.9 GPa	216 GPa
Poisson's Ratio	0.33	0.26
Mass Density	2710 kg/m^3	7825 kg/m^3

The chamber was modeled as a thin spherical shell, with no perforations for this initial scoping study. For the mechanical analysis, the motion is completely symmetric, i.e., the shell is always spherical and simply expands and contracts with the same radial displacement component everywhere on the sphere. The natural vibration frequency in this case depends upon the elastic modulus, density, Poisson's ratio and the shell radius but is independent of the thickness. An impulsive pressure will develop dynamic stresses which are independent of radius and are essentially the same for 2.25 Cr - 1 Mo steel and 6061 aluminum because of similar material property ratios [4.3]. The equations of motion of a sphere were solved with a Runge-Kutta algorithm using the results of the CONRAD simulations as the loading. A damping level of 2% was used for all cases. Figures 4.4 and 4.5 show the calculated wall stresses for the two chambers (1.0 m and 0.5 m radii, respectively), using the impulsive pressures and afterpressures given in Table 4.2. The results are valid for both Al 6061 and 2.25 Cr - 1 Mo and for wall thicknesses of 1.25 cm, 2.5 cm and 5.0 cm. The effect of the afterpressure can easily be seen in each case. In addition, all stresses calculated were a fraction of the yield stress of the two materials, so it was predicted that the APEX chamber would easily survive a single shot.

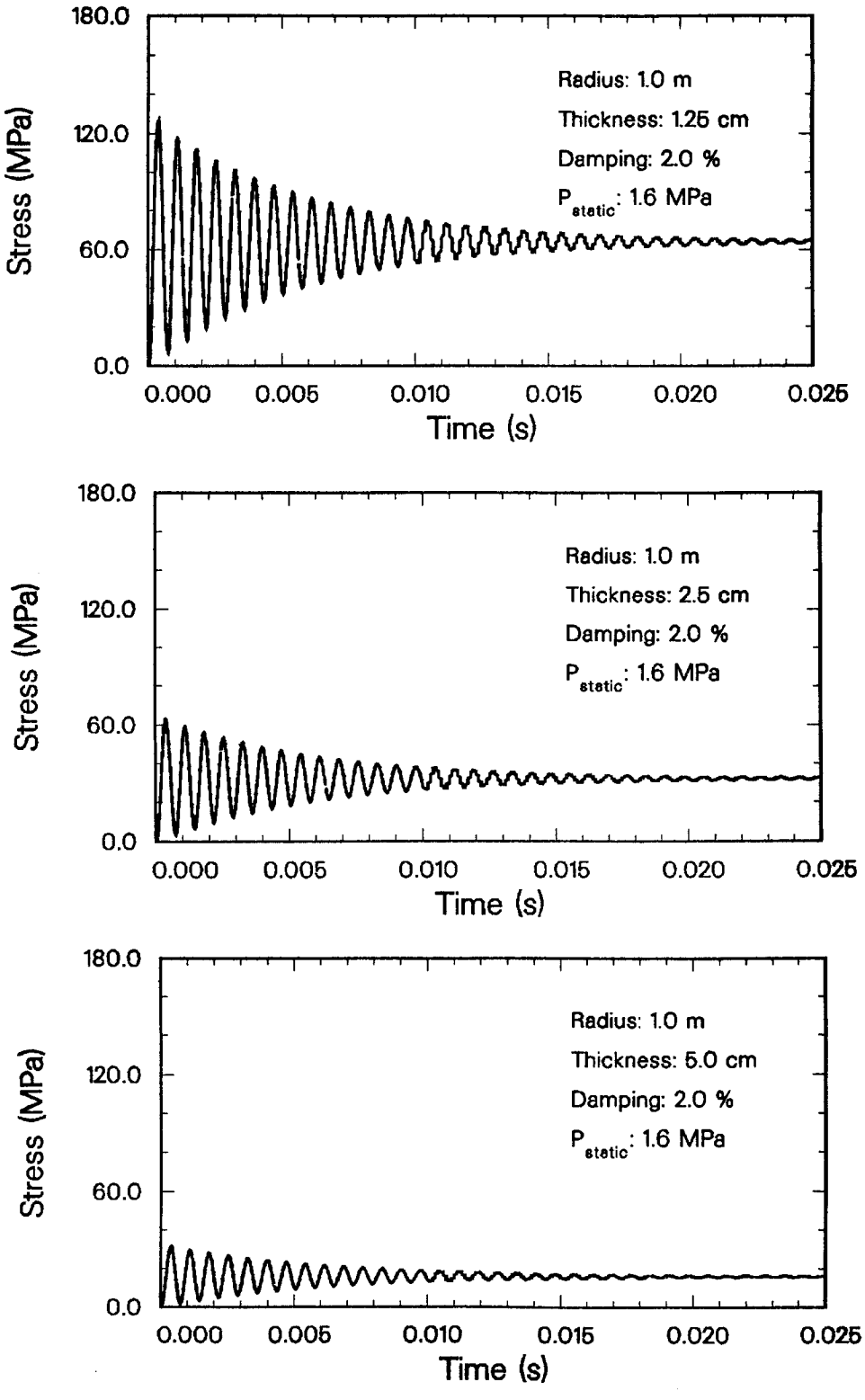

Fig. 4.4. Mechanical stress history of the APEX target chamber (1.0 m radius).

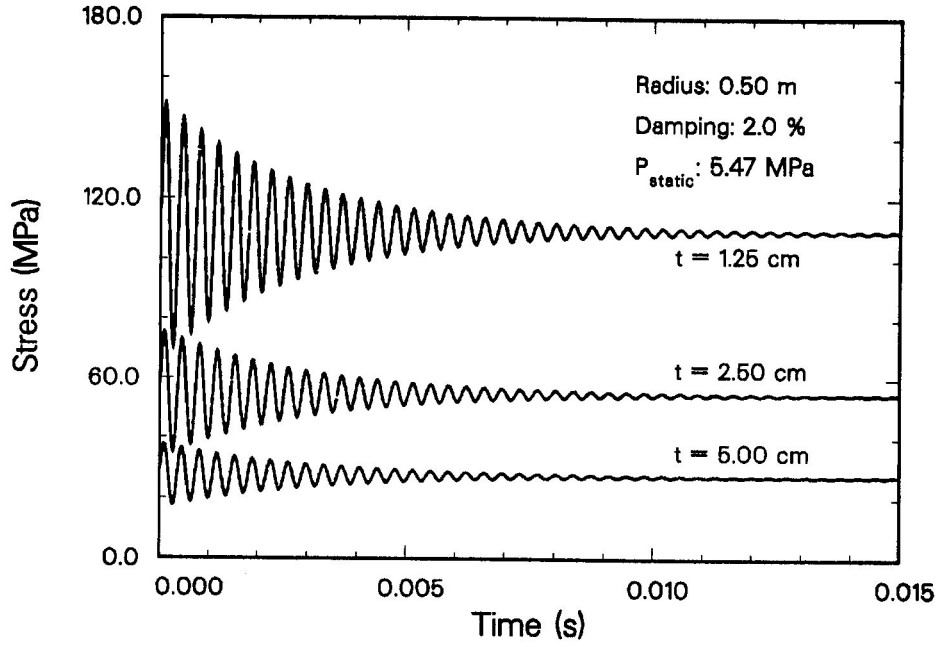

Fig. 4.4. Mechanical stress history of the APEX target chamber (0.5 m radius).

Further details on the design and analysis of the APEX target chamber can be found in References [4.4] and [4.5].

4.4 References

[4.1] R. R. Peterson, "CONRAD - A Combined Hydrodynamics-Vaporization/ Condensation Computer Code," UWFDM-670, University of Wisconsin Fusion Technology Institute Report, 1986.

[4.2] Nuclear Materials System Handbook, Material Property Data.

[4.3] E. Lovell, University of Wisconsin - Madison, private communication.

[4.4] R. Peterson, R. Engelstad, G. Moses and E. Lovell, "Target Chamber Design Considerations for the APEX Light Ion Beam Fusion Facility," UWFDM-724, University of Wisconsin Fusion Technology Institute Report, 1987.

[4.5] G. Moses et al., "Design Studies of the APEX Light Ion Fusion Experiment," UWFDM-735, University of Wisconsin Fusion Technology Institute Report, 1987.

5. LABORATORY MICROFUSION FACILITY (LMF)

5.1 LMF Target Chamber Parameters and Conditions

Two target chamber designs (shown in Fig. 5.1) were considered for the light ion LMF. Both designs consisted of a cylindrical shell (with either a 1.5 m or 3.0 m radius) with end caps to provide extra volume for any residual overpressure. For shielding, each had a Boral liner on the outside surface of the chamber wall and a borated water filled tank surrounding the entire chamber. The relative features of the target chamber, water shield and beam lines are illustrated in Fig. 5.2, using the 1.5 m radius chamber as an example. The principal mechanical parameters of the two chambers are given in Table 5.1. As listed in the table, both designs employ a liner made of woven carbon/carbon composite to protect the first wall from the intense thermal load and target debris. Compared with traditional graphites, such composites have a higher resistance to crack growth and a reduced solid density which better accommodates transient thermal strains. Weaves with fibers through the thickness raise delamination thresholds from shock and in addition the composites can be fabricated into complex configurations.

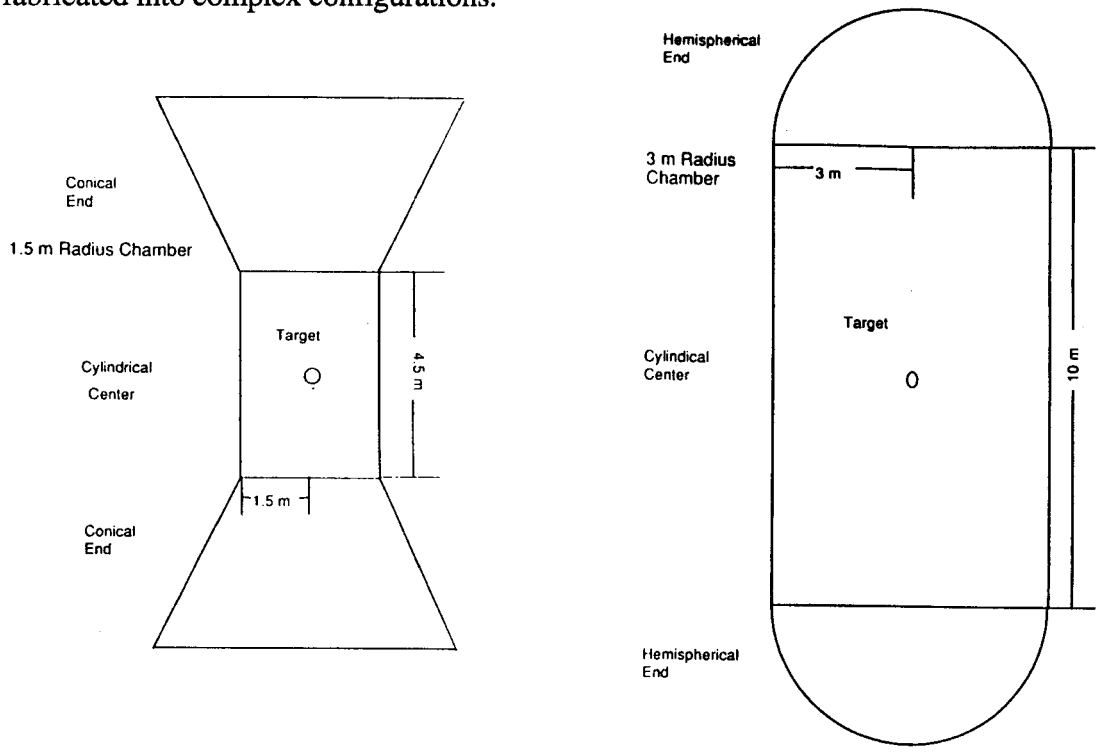

Fig. 5.1. Two target chamber designs for the light ion fusion LMF.

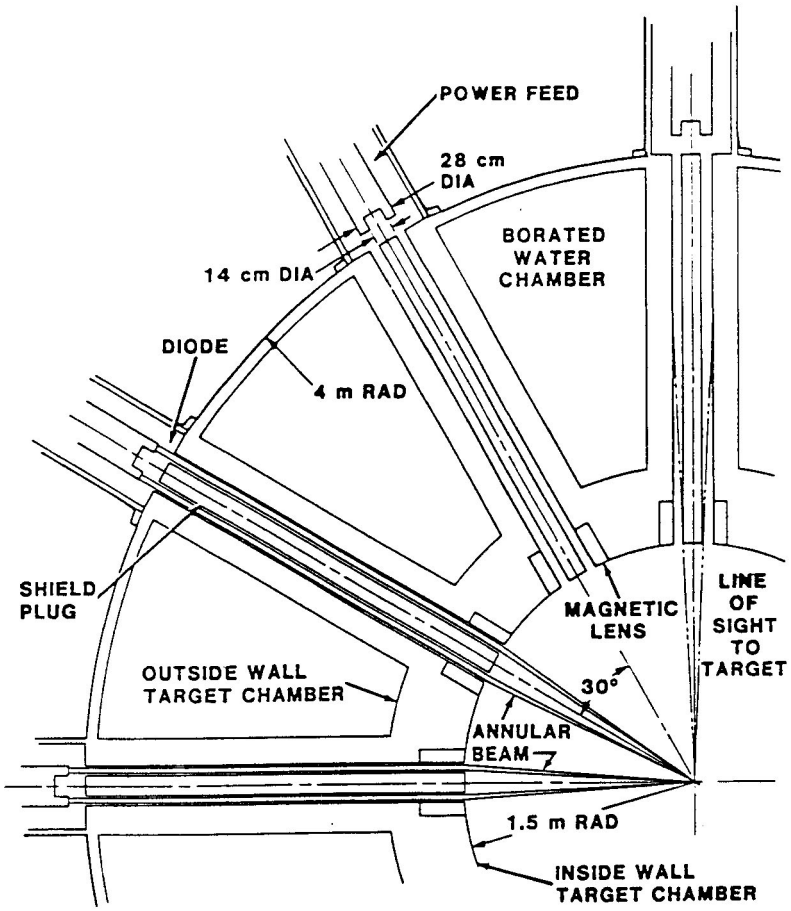

Fig. 5.2. Overhead view of the light ion fusion LMF target chamber.

Table 5.1. Mechanical Parameters for the LMF Chamber.

Geometry	Capped Cylindrical Shell
Radius	1.5 m or 3.0 m
Cylindrical Wall Height	4.5 m or 10.0 m
Maximum Unsupported Wall Height	4.5 m (both)
Number of Beam Ports	36
Port Diameters	36 cm
Fill Gas	1 torr He
Thermal Liner Thickness	2 cm
Thermal Liner Material	Carbon/carbon composite
Structural Materials	Al 6061-T6, or 2.25 Cr - 1 Mo Steel

Considerng the chamber itself, both designs have an unsupported wall height of 4.5 m with 3 circumferential rows of beam ports having 12 ports per row. It can be seen from Fig. 5.3 that the shell appears highly perforated, requiring an assessment of reduced stiffness and increased stress in these regions. To account for this effect, modified elastic constants were used in place of actual material properties, e.g., Young's modulus and Poisson's ratio. This was done for both the triangular and square perforation patterns shown in Fig. 5.3. Details of this procedure are given in Section 5.3 of this report.

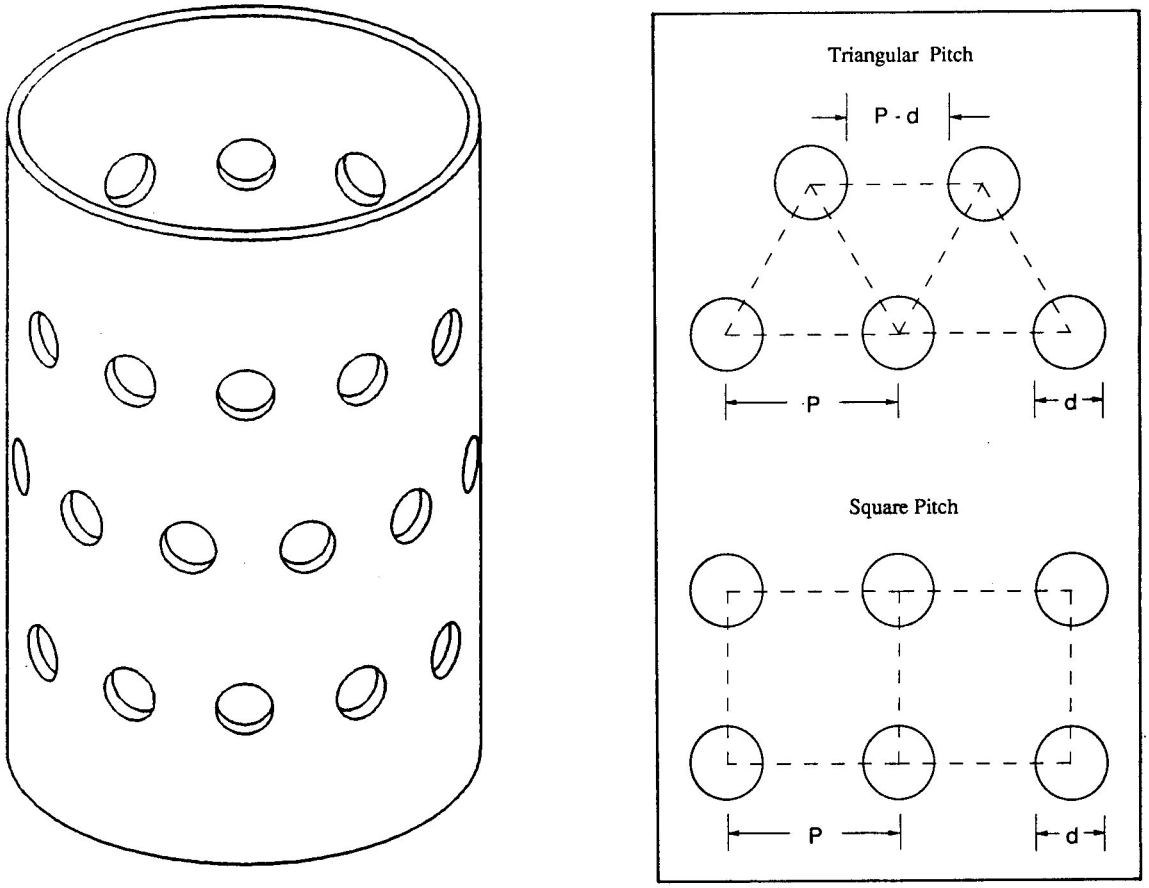

Fig. 5.3. Cylindrical target chamber with a schematic of the perforation patterns.

5.2 Hydrodynamics

The LMF target chamber analysis considered blast loadings with target yields ranging from 10 to 1000 MJ. These pressure loads consisted of two components: an initial pressure spike caused by the rapid x-ray vaporization of the first wall surface and a residual afterpressure due to the resulting energy content of the vapor and the target chamber gas.

The hydrodynamics code CONRAD [5.1] was used to calculate the initial pressure loading. For example, Fig. 5.4 shows the load history for a 1000 MJ target yield where the duration of the initial spike is on the order of a few nanoseconds. Thus, when compared with the response time of the shell (or the natural period of vibration), the loading could be characterized by an impulse. In addition to this initial impulse, a steady afterpressure of a sizable amount followed. Table 5.2 shows the pressure loadings considered in this analysis for various target yields at the two different radii. The residual pressures, also referred to as $P_{static,}$ were computed from $(\gamma\text{-}1)E/V$ where γ is the ratio of specific heats for the gas, E is the thermal energy in the gas and V is the gas volume.

Table 5.2. Pressure Loadings on the LMF Chamber.

Case I: Radius = 1.5 m

Target Yield (MJ)	Impulsive Pressure (Pa-s)	Residual Pressure P_{static} (MPa)
1000	284	0.77
200	55	0.22
50	10	0.062
10	0.7	0.0062

Case I: Radius = 3.0 m

Target Yield (MJ)	Impulsive Pressure (Pa-s)	Residual Pressure P_{static} (MPa)
1000	84.5	0.3310
200	14.9	0.0733
50	2.13	0.0145
10	0.11	0.0018

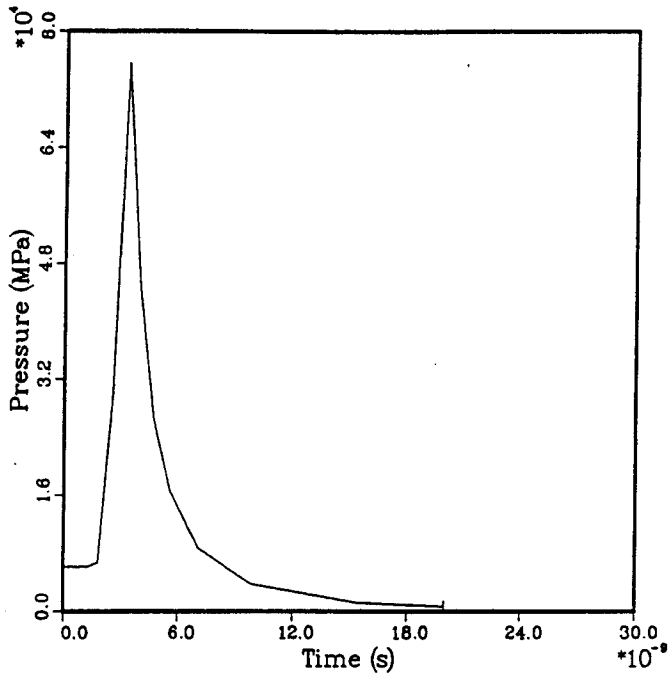

Fig. 5.4. Pressure history at 1.5 m radius chamber wall for 1000 MJ yield.

The actual shape of the pressure versus time curve after the initial spike could not be fully identified. A worst case model of the afterpressure would be a dynamic step function which is superimposed with the impulse load (see Fig. 5.5). However, a more accurate representation of the afterpressure history would be a "ramped step" such as the model shown in Fig. 5.6. The CONRAD code was used to predict the times t_2 and t_3, which characterize this ramp loading. For example, for the chamber of radius 1.5 m, t_2 is approximately 0.1 ms and t_3 is 0.8 ms; for the chamber of radius 3.0 m, t_2 is 1.07 ms and t_3 is 1.32 ms.

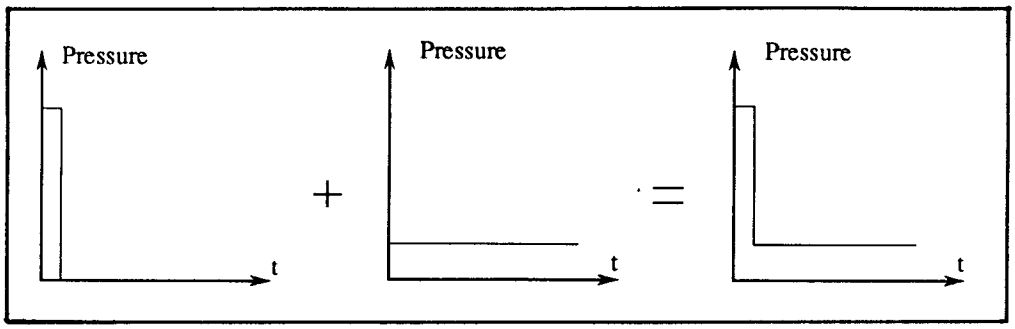

Fig. 5.5. Typical impulse superimposed with a step load.

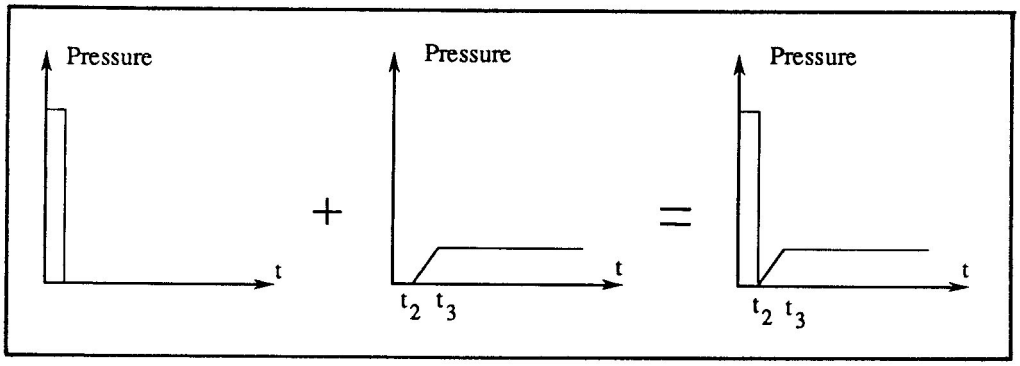

Fig. 5.6. Typical impulse superimposed with a ramped step load.

5.3 Mechanical Response

The pressure loads were assumed to be uniformly distributed over the first wall of the chamber, resulting in an axisymmetric mechanical response that is also symmetric with respect to the midspan plane. The target chamber was modeled as a thin-walled cylindrical shell with clamped boundary conditions at both ends. In addition, it was assumed to be restrained from expanding axially. The largest stresses in the cylinder will occur (due to bending) at the location of the rigid end supports. However, localized thickening of the chamber walls in this region could control these stresses; therefore, the shell design was based on the minimum thickness needed at the midspan. It was also assumed that the longitudinal (or axial) stress was zero at the midspan, resulting in a uniaxial state of stress (in the circumferential direction) at this location.

Two materials were considered in the structural analysis of the LMF chamber, i.e., 2.25 Cr - 1 Mo and 6061-T6 aluminum (unwelded and welded). The aluminum alloys were considered in order to minimize the radiological dose near the chamber during the initial period after operation. The 2.25 Cr - 1 Mo steel was a candidate material because it had been widely used in conventional nuclear installations and thus had well-documented characteristics. Basic mechanical properties of these alloys can be found in Table 5.3 [5.2, 5.3].

Table 5.3. Static Properties of Chamber Materials.

	Unwelded Al 6061 - T6	Steel 2.25 Cr - 1 Mo
Yield Strength	103 MPa	206 MPa
Ultimate Strength	166 MPa	415 MPa
Elastic Modulus	68.9 GPa	216 GPa
Poisson's Ratio	0.33	0.26
Mass Density	2710 kg/m^3	7825 kg/m^3

To show the effects of the various types of pressure loadings described above, an unperforated steel chamber with a radius of 1.5 m and a thickness of 5.0 cm was used. Figure 5.7 shows the circumferential stress history at the midspan of the chamber caused by a single impulsive load of 284 Pa-s (corresponding to a 1000 MJ yield). From the plot it can be seen that the impulse causes the chamber to oscillate about the zero stress axis, producing maximum stresses around 30 MPa. The 2% damping assumed for the chamber causes these stresses to approach zero in a very short time. The circumferential stresses that result from a single step load with a magnitude of 0.77 MPa are shown in Fig. 5.8. If allowed to damp completely, the final stress level will match that given by a 0.77 MPa static pressure. To determine the response of the chamber to the combined effects of impulsive and step loads, i.e., as in Fig. 5.5, the results from the two separate load cases are superimposed. The total stress history resulting from a 284 Pa-s pressure pulse and a 0.77 MPa afterpressure is shown in Fig. 5.9. The combined dynamic effects produced a rather severe response, driving the peak stress to over 60 MPa. However, it was assumed that the actual pressure loading would be better characterized by an impulse with a ramped step (as shown in Fig. 5.6). Figure 5.10 shows the response of the same chamber using a 284 Pa-s impulse superimposed with a ramp that starts at 0.1 ms and reaches 0.77 MPa at 8 ms. Since the ramped step load is less severe than the step, the magnitude of the oscillations is somewhat smaller. In addition, the response of the impulse alone is slightly out of phase from the response of the ramped step, causing a reduction in the total stress when the two are superimposed. It should be noted, however, that the phase shift depends on the ramp times t_2 and t_3 relative to the period of the shell.

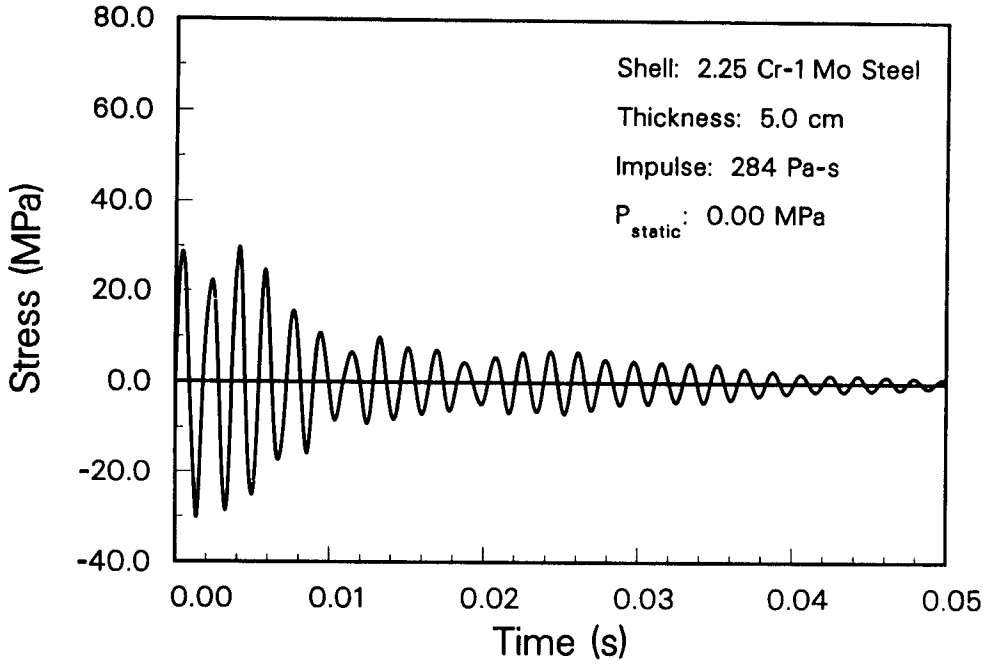

Fig. 5.7. Circumferential stresses produced by an impulsive load.

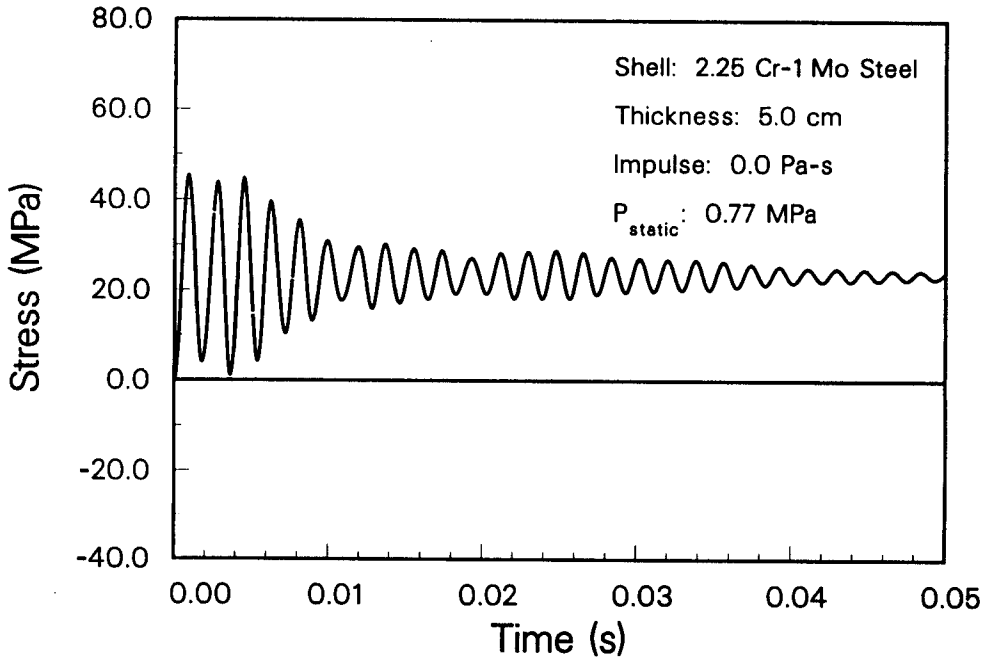

Fig. 5.8. Circumferential stresses produced by a step load with a magnitude of 0.77 MPa.

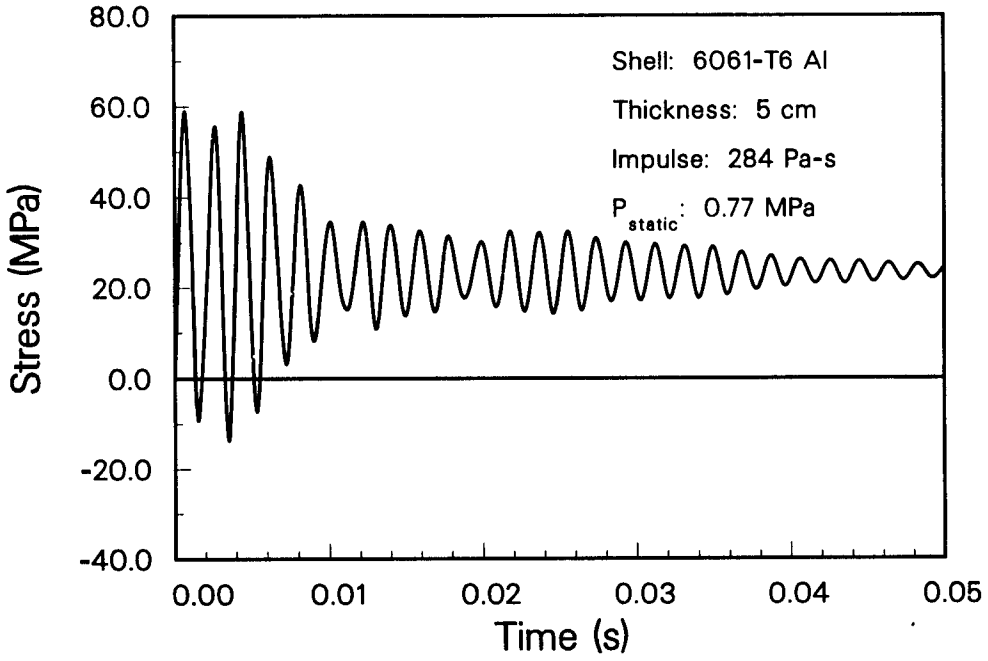

Fig. 5.9. Circumferential stresses produced by an impulsive load superimposed with a step load.

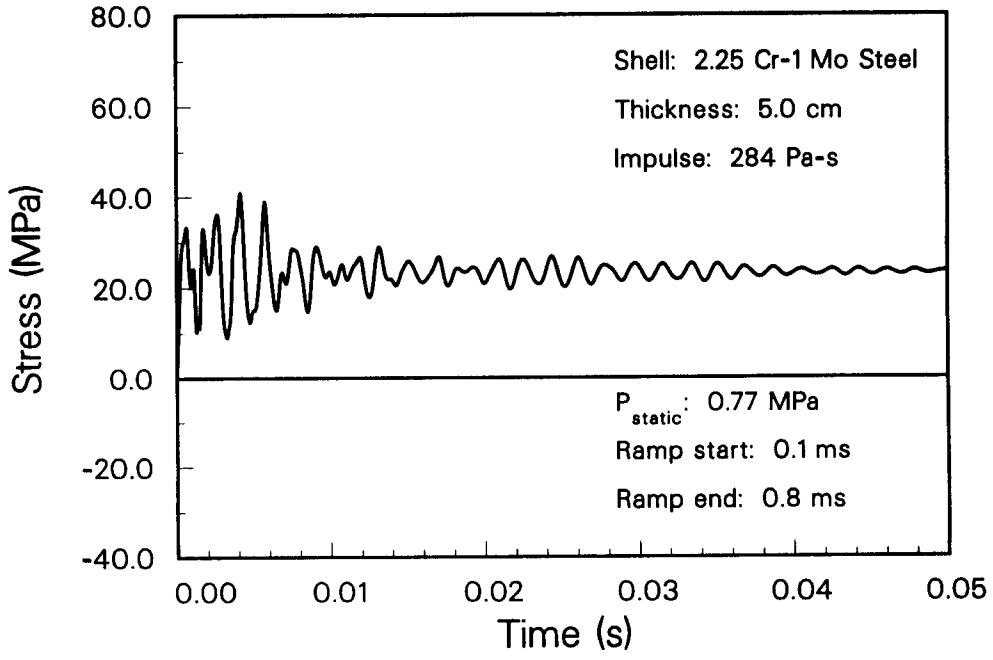

Fig. 5.10. Circumferential stresses produced by an impulsive load superimposed with a ramped step load.

Comparing the dynamic response from each load type, the importance of including the afterpressure in all fatigue calculations is obvious. What may seem like a relatively insignificant residual pressure, may actually produce a substantial mean stress in addition to amplifying the alternating stress. The rise time of the ramp is also an important parameter affecting the magnitude and general characteristics of the response. If a means were devised of venting the afterpressure so that the rise time was increased and the peak static pressure was decreased, the actual strains and stresses developed in the chamber would be substantially reduced.

In order to account for the weakening effect of the shell perforations on the mechanical response of the chamber's wall, modified effective elastic constants were used in place of actual material properties. These equivalent efficiency factors have been successfully used for years in the design of perforated tube-sheets and tube-plates [5.4, 5.5, 5.6]. The method has been extended to the research here with the intent of determining an equivalent solid cylinder that could be analyzed by conventional shell equations. Two types of perforation patterns were considered, i.e., triangular and square. These are shown in Fig. 5.3 with the pitch P defined as the distance between perforation centers and the ligament efficiency μ defined as 1.0 - (d/P) where d is the diameter of the perforation. With the numerical data for specific geometries being somewhat limited, ligament efficiencies of 0.33 and 0.40 were used for the triangular and square perforation patterns, respectively. For the configuration and geometry of the LMF chamber, μ was actually 0.54. Thus the design was considered to be on the conservative side. In fact, with the lower ligament efficiencies used in the calculations, the design was comparable to a chamber with up to 15 beam ports (36 cm in diameter) in each of the 3 tiers, instead of the actual 12. Figure 5.11 shows the data used for both the elastic modulus E* and Poisson's ratio ν*, as a function of the wall thickness, h [5.4]. It is these curves which are programmed into the structural response and fatigue code.

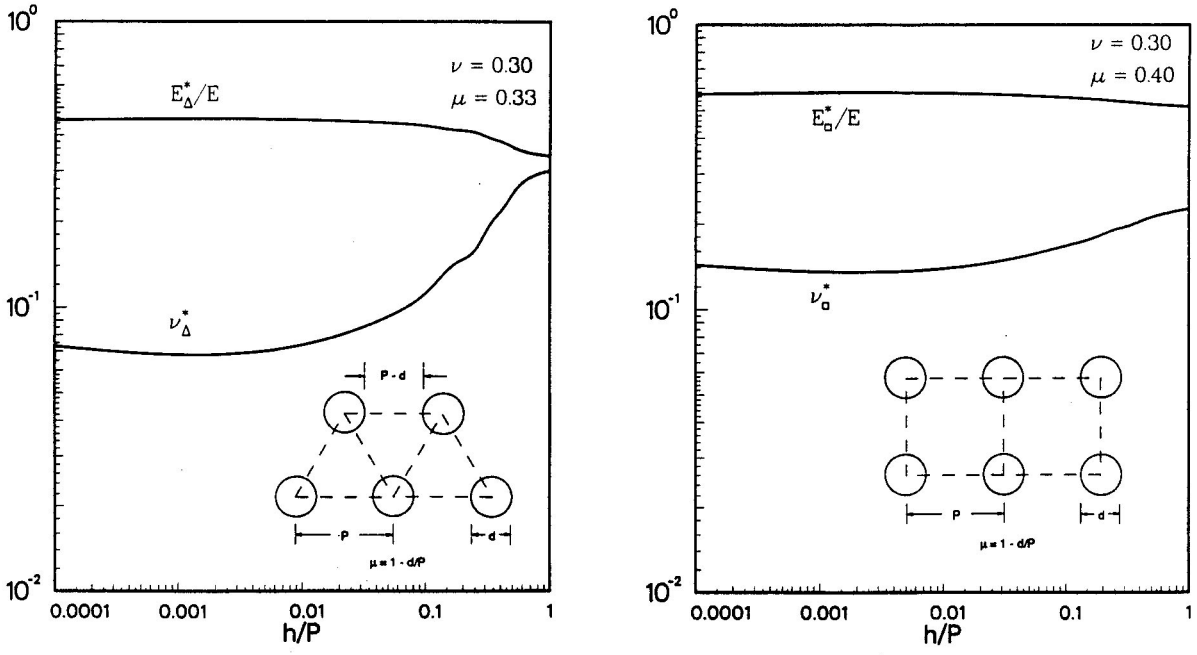

Fig. 5.11. Effective elastic constants for triangular and square perforation patterns.

5.4 Chamber Lifetime Analysis

Cumulative damage was used in the fatigue analysis since each stress/strain history was characterized by cycles of different amplitude and each target yield produced a different history. Because of the mean stresses/strains present in addition to the alternating stresses/strains, an appropriate cycle counting method was used to determine an equivalent history that could be evaluated with the constant amplitude, fully reversed fatigue data. One of the most widely accepted techniques, and one of the most accurate, is the rainflow method. The algorithm used to perform the rainflow cycle counting was taken from the recommended procedures published by the American Society of Testing and Materials (ASTM) [5.7]. A Goodman diagram was used in conjunction with the cycle counting in order to obtain the value of the equivalent range stress/strain. Finally, Miner's rule was applied to estimate the linear, cumulative damage effects. It should be noted that this procedure (for the fatigue lifetime calculations) is consistent with the intent and methodology of the ASME Pressure Vessel Code [5.8, 5.9]. Safety factors of either two on stress/strain or twenty on cycles is specified by the code; however, for the type of loading conditions on the LMF chamber, a factor of safety of two was more conservative.

Two materials were considered in the structural analysis of the LMF chamber, 2.25 Cr - 1 Mo steel and 6061-T6 aluminum. Figure 5.12 shows the strain-based fatigue data for 2.25 Cr - 1 Mo that were published by Booker et al., at ORNL [5.10] The data were obtained from completely reversed loadings with constant amplitude strains applied at the rate of 4×10^{-1}/s. The latest fatigue data on welded Al 6061-T6 were obtained from the Aluminum Association and is shown in Fig. 5.13 [5.11]. The data (stress-based) were given for "Category B" type welded joints. The lower 95% confidence limit, as shown on the curve, was used in all fatigue calculations. In addition, the Aluminum Association recommends that the maximum range stress should not exceed 12.0 ksi (82.8 MPa).

Fatigue calculations were carried out for lifetimes of 3, 6, 9, 12 and 30 years. Table 5.4 shows the cumulative shots for each of the target yields considered. The results of the fatigue calculations were governed by the loadings of the 1000 MJ shots for both the steel and the aluminum, with the primary failure mode being yielding. Thus the value of the thickness remains the same for lifetimes of 6, 9, 12 and 30 years in each case. However, with no 1000 MJ shots present in the first 3 years, the value of the minimum thickness drops significantly. For example, Table 5.5 gives the chamber thicknesses needed for a 3 year lifetime, while Table 5.6 provides the results for the 6, 9, 12 and 30 year lifetimes. The effect of using the ramped step load model is also reflected in the required values of the thicknesses, i.e., substantial reductions can be seen. It should also be noted that a number of the fatigue calculations show that the chamber can be built with relatively thin walls depending on the material, lifetime, etc. Since buckling becomes an issue for thin shells, a 3 cm lower limit is recommended for the chamber wall thickness in all cases unless additional reinforcements of the structure are used.

Further details on the design and analysis of the LMF target chamber can be found in References [5.12] to [5.15].

Table 5.4. LMF Cumulative Shots Required.

Years of Operation	Target Yield			
	10 MJ	50 MJ	200 MJ	1000 MJ
3	990	480	30	0
6	1800	1080	90	30
9	1950	2130	330	90
12	2010	2970	810	210
30	2190	5490	5850	1470

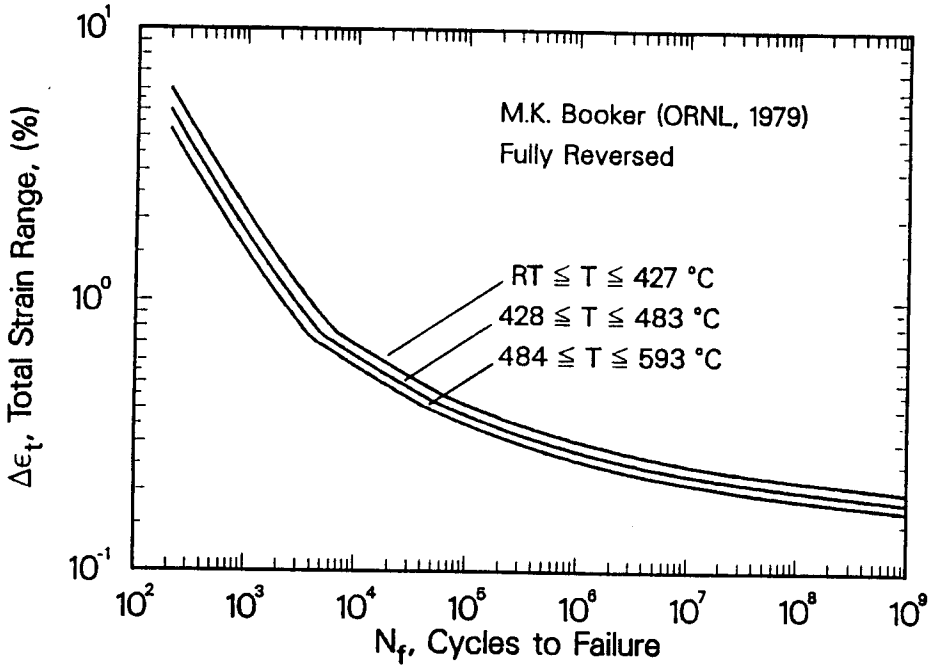

Fig. 5.12. Fatigue data for 2.25 Cr - 1 Mo steel.

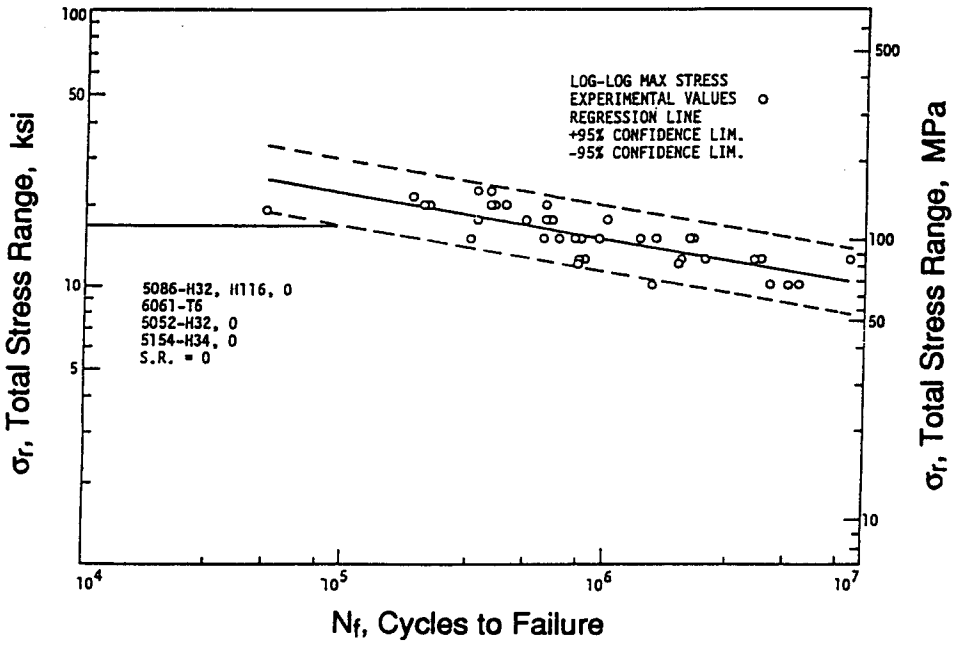

Fig. 5.13. Fatigue data for welded 6061-T6 aluminum.

Table 5.5. Minimum Thicknesses Needed for a Lifetime of 3 Years.

Case I: Radius = 1.5 m

Material	Port Pattern	Minimum Thickness (cm) Impulse + Step	Minimum Thickness (cm) Impulse + Ramped Step
Steel	Unperforated	0.7	0.4
Steel	Square	1.2	0.7
Steel	Triangular	1.5	1.1
Al (unwelded)	Unperforated	1.8	0.8
Al (unwelded)	Square	2.7	1.7
Al (unwelded)	Triangular	3.6	2.6
Al (welded)	Unperforated	1.9	0.9
Al (welded)	Square	2.9	1.8
Al (welded)	Triangular	3.9	2.7

Case II: Radius = 3.0 m

Material	Port Pattern	Minimum Thickness (cm) Impulse + Step	Minimum Thickness (cm) Impulse + Ramped Step
Steel	Unperforated	0.5	0.4
Steel	Square	0.5	0.4
Steel	Triangular	0.5	0.4
Al (unwelded)	Unperforated	1.0	0.9
Al (unwelded)	Square	1.0	0.9
Al (unwelded)	Triangular	1.0	0.9
Al (welded)	Unperforated	1.1	0.9
Al (welded)	Square	1.1	0.9
Al (welded)	Triangular	1.1	0.9

Table 5.6. Minimum Thicknesses Needed for a Lifetimes of 6, 9, 12, and 30 Years.

Case I: Radius = 1.5 m

Material	Port Pattern	Minimum Thickness (cm) Impulse + Step	Minimum Thickness (cm) Impulse + Ramped Step
Steel	Unperforated	2.9	1.6
Steel	Square	4.5	2.5
Steel	Triangular	6.1	3.7
Al (unwelded)	Unperforated	7.2	3.9
Al (unwelded)	Square	11.3	4.8
Al (unwelded)	Triangular	15.6	8.0
Al (welded)	Unperforated	8.3	4.3
Al (welded)	Square	13.0	4.8
Al (welded)	Triangular	20.7	10.8

Case II: Radius = 3.0 m

Material	Port Pattern	Minimum Thickness (cm) Impulse + Step	Minimum Thickness (cm) Impulse + Ramped Step
Steel	Unperforated	2.0	1.6
Steel	Square	2.0	1.6
Steel	Triangular	2.0	1.6
Al (unwelded)	Unperforated	4.6	3.7
Al (unwelded)	Square	4.6	3.8
Al (unwelded)	Triangular	4.6	3.8
Al (welded)	Unperforated	4.9	4.0
Al (welded)	Square	4.9	4.0
Al (welded)	Triangular	4.9	4.0

5.5 References

[5.1] R. R. Peterson, J. J. MacFarlane and G. A. Moses, "CONRAD - A Combined Hydrodynamics-Condensation/Vaporization Computer Code," UWFDM-670, University of Wisconsin Fusion Technology Institute Report, 1986, revised 1988.

[5.2] Engineering and Design Task Force, "Specifications for Aluminum Structures," *Aluminum Construction Manual*, Fifth Edition, The Aluminum Association, Washington, DC, 1986.

[5.3] ASTM Committee A-1 on Steel, "Standard Specification for Pressure Vessel Plates, Alloy Steel, Chromium-Molybdenum," Designation A 387/A387M-89, *1990 Annual Book of ASTM Standards*, American Society for Testing and Materials, Easton, MD, Vol. 1.04, pp. 257, 1990.

[5.4] F. Osweiller, "Evolution and Synthesis of the Elastic Constants, Concept from 1948 to Present - New Design Curves for Triangular and Square Patterns," *Design and Analysis of Piping, Pressure Vessels, and Components*, Proceedings of the 1987 Pressure Vessels and Piping Conference, Vol. 120, pp. 137, 1987.

[5.5] P. Meijers, "Refined Theory for Bending and Torsion of Perforated Plates," *Pressure Vessel Components Design and Analysis*, Proceedings of the 1985 Pressure Vessels and Piping Conference, Vol. 98, pp. 11, 1985.

[5.6] W. O'Donnell, "Perforated Plates and Shells," *Pressure Vessels and Piping: Design and Analysis a Decade of Progress*, ASME, New York, NY, 1972.

[5.7] ASTM Committee E-9 on Fatigue, "Standard Practices for Cycle Counting in Fatigue Analysis," *1988 Annual Book of ASTM Standards*, Designation: E 1049-85, American Society for Testing and Materials, Vol. 3.01, pp. 764, 1990.

[5.8] ASME Boiler and Pressure Vessel Code, Section III, Nuclear Power Plant Components, 1986.

[5.9] ASME Boiler and Pressure Vessel Code, Case Interpretations, Code Case N-47, 1974.

[5.10] M. K. Booker, J. P. Strizak and C. R. Brinkman, "Analysis of the Continuous Cycling Fatigue Behavior of 2.25 Cr-1 Mo Steel," Oak Ridge National Laboratory Report ORNL-5593, Oak Ridge, TN, 1979.

[5.11] W. W. Sanders, Jr. and J. W. Fisher, "Development of Recommended Specifications for Fatigue Design of Aluminum Structures," Aluminum Association, October, 1985.

[5.12] R. Peterson et al., "An Overview of Target Chamber Design and Analysis for the Light Ion Beam Laboratory Microfusion Facility," UWFDM-819, University of Wisconsin Fusion Technology Institute Report, 1990.

[5.13] R. Engelstad, J. Powers and E. Lovell, "Mechanical Design of the LMF Target Chamber," UWFDM-828, University of Wisconsin Fusion Technology Institute Report, 1990.

[5.14] R. Peterson et al., "Target Chamber Issues for the Sandia National Laboratories Laboratory Microfusion Facility - Final Report for the Period 10/1/88 through 12/31/90," UWFDM-854, University of Wisconsin Fusion Technology Institute Report, 1991.

[5.15] J. Powers, "Structural and Fatigue Analysis of the Sandia Laboratory Microfusion Reactor Chamber," M.S. Thesis, Mechanical Engineering Department, University of Wisconsin - Madison, 1991.

6. NATIONAL IGNITION FACILITY (NIF)

6.1 NIF Target Chamber Parameters and Conditions

The proposed design for the NIF target chamber [6.1, 6.2] is a spherical aluminum shell, 10 m in diameter and 10 cm thick. The interior of the target chamber will be covered by replaceable, first wall panels that provide a protective layer to soft x-rays and shrapnel. These panels will be approximately 1.0 cm in thickness and will cover roughly 85% of the chamber, leaving openings for all ports. The construction of the panels calls for a 0.95 cm thick substrate using aluminum 5083, coated with a 0.05 cm thick layer of boron. The target chamber will maintain a 1×10^{-5} torr vacuum during operation with the outer aluminum shell providing a mounting surface for the first wall panels and, in addition, serving as a vacuum barrier.

The target chamber and the first wall will need to accommodate holes (or ports) for the 192 laser beams, the target diagnostics and the vacuum pumps. The laser beams will enter the spherical chamber in conical arrays from the top and bottom through final optic packages mounted to the target chamber. However, it is worth noting that the placement of the laser ports in conjunction with the diagnostic ports results in a nonsymmetric design of the chamber sphere. This obviously increases the difficulty in characterizing the overall chamber response under dynamic loading.

A pressure versus time history has been computed, with the shape of the pulse essentially given by a spike with an exponential decay. The peak pressure at the chamber wall, 5.0 m away, has been calculated at 14.5 bar for a 30 MJ yield target. The duration of this pressure impulse is on the order of 40 μs. Thermal loading has not yet been reported.

The spherical target chamber will be housed in a reinforced concrete building. The chamber itself will be supported using a combination of a pedestal (a hollow cylinder positioned directly below the chamber) and spoke supports (attached to the sides). The concrete and aluminum pedestal will carry the vertical loads and the spokes will provide restraint from both torsional and horizontal loads. In addition, the spokes will contain the vibration isolation system to help maintain the stability of the target chamber. This is necessary for beam alignment purposes and for controlling ambient random vibration.

A static structural analysis of the target chamber has already been completed using finite element methods. Maximum stresses and deflections, along with buckling loads, have been completed which include the static loads from the chamber itself, first wall, external shielding, diagnostic equipment and final optics equipment. Scientists at LLNL reported

that the maximum stress in the chamber was approximately 32 MPa. However, the dynamic stress analysis of the chamber wall has not been completed. In fact, Peter Cousseau from the University of Wisconsin - Madison may soon be working on structural dynamics issues if his summer internship with LLNL is granted. The dynamic response of the chamber will obviously dictate the final design on vibration isolation system.

6.2 NIF Minichamber Parameters and Conditions

The NIF minichamber is a concept proposed by Prof. Per Peterson at the University of California at Berkeley for basic diagnostic testing. The minichamber is a smaller chamber that is to be inserted inside the main NIF target chamber through the hollow cylinder used for the pedestal support. With this design constraint, the proposed minichamber would be approximately one tenth the size of the main chamber. The target would be contained inside the minichamber and both would be cryogenically cooled.

As of the end of 1995, the final configuration of the minichamber had not yet been established. Possible design options included a spherical chamber or a cylindrical chamber with hemispherical end caps. It would be constructed out of aluminum with perforations to allow the laser beams to reach the target. To investigate the feasibility of the minichamber withstanding a typical blast loading, a scoping study was performed by scientists at the University of Wisconsin - Madison in conjuction with Prof. Peterson. For convenience, the chamber was assumed to be cylindrical in shape with no perforations (a worst case scenario). In addition, no supporting structure or constraints were placed on the sphere. The outer radius was assumed to be 55 cm and the thickness was set at 5 cm (but could be varied as needed).

6.3 Hydrodynamics

Figure 6.1 shows the time dependent pressure load calculated by Prof. Per Peterson and his graduate student John Scott at the University of California at Berkeley using the code TSUNAMI. (Details on the target itself are not known.) It is assumed that the pressure is applied uniformly on the inside of the sphere, normal to the surface. The maximum pressure of 2.66 MPa occurs at 4.3 μs, then at 100 μs the pressure decays away

until it reaches zero at 1 ms. For convenience, a linear function was assumed for the decay beyond 100 μs.

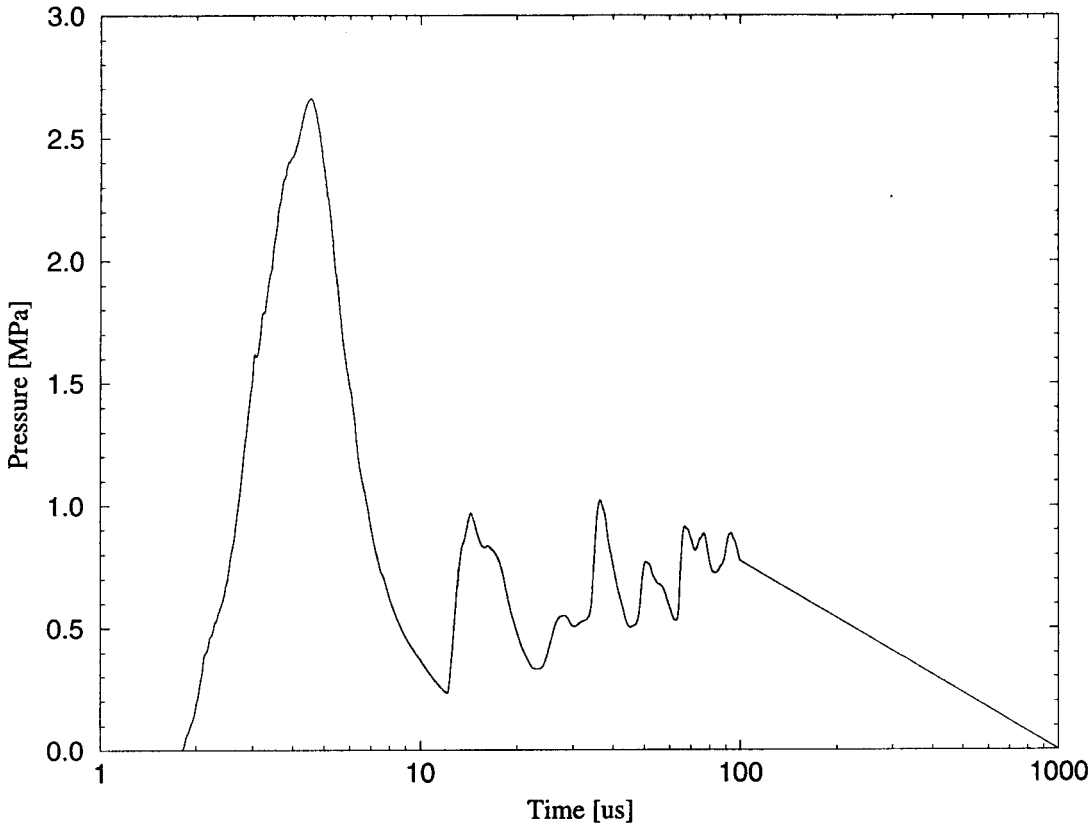

Fig. 6.1. Internal pressure loading on the NIF minichamber (P. Peterson and J. Scott).

6.4 Mechanical Response

The minichamber was modeled as a homogenous, thin, spherical shell with no perforations or supporting structure, i.e., no boundary conditions were applied. Both analytical and numerical analyses were completed. The effects of material properties have not been fully assessed, since for this case the aluminum chamber is to be kept at cryogenic temperatures. Table 6.1 lists the material properties of 6061 aluminum at room temperature [6.3]. However, at a temperature of -240 □C, the yield strength increases from 270 MPa to 340 MPa and the ultimate strength (or tensile strength) increases from 310 MPa to 480 MPa [6.4]. Therefore, for this scoping study, the more conservative properties were used in the

analyses, i.e., those at room temperature. In addition, a structural damping level of 1.0% was set for all calculations.

Table 6.1. Material Parameters for 6061 Aluminum at Room Temperature

Yield Strength	270 MPa
Ultimate Strength	310 MPa
Modulus of Elasticity	70 GPa
Density	2700 kg/m^3
Poisson's Ratio	0.33
Structural Damping	1.0%

An axisymmetric finite element model of a sphere was constructed using ANSYS, a commercially available finite element package. The shell elements used in the analysis included both bending and membrane stiffness. A transient solution was employed to calculate the displacements and stresses as a function of time due to the time dependent pressure loading.

An analytical solution for the response of the minichamber to an impulse loading was also examined. Reference [6.5] presents the axisymmetric equation of motion of a thin, spherical shell with free boundary conditions. The theoretical solution also neglects bending stiffness (i.e., provides only a membrane approximation). Using the convolution integral, the impulse solution with the pressure load was numerically integrated to find the response of the shell. Figure 6.2 shows the analytical results for the radial displacement of the shell during and after the impulsive pressure loading. For a thickness of 5 cm, a maximum radial displacement of 0.0385 mm occurs at 0.19 ms. The figure shows the shell "ringing" or vibrating for 20 to 30 ms after the end of the pressure loading. The duration of the "ringing" is directly affected by the amount of structural damping in the system.

Figure 6.3 compares the analytical and finite element solutions for the in-plane or membrane stress in the shell during the first 0.20 ms of the pressure loading. A maximum stress of 7.7 MPa occurs at 0.19 ms (the same time as the maximum radial displacement). The remainder of stress history will follow the same characteristic curve as the displacements. In addition, the finite element model is capable of calculating the stress at both the inner and outer surfaces of the shell, which can be seen in Fig. 6.3. Note that as the impulse load is first applied, the shell cannot respond in the same time frame. In fact, on the

inner surface of the shell a compressive stress develops because the shell itself is effectively behaving as a constraint.

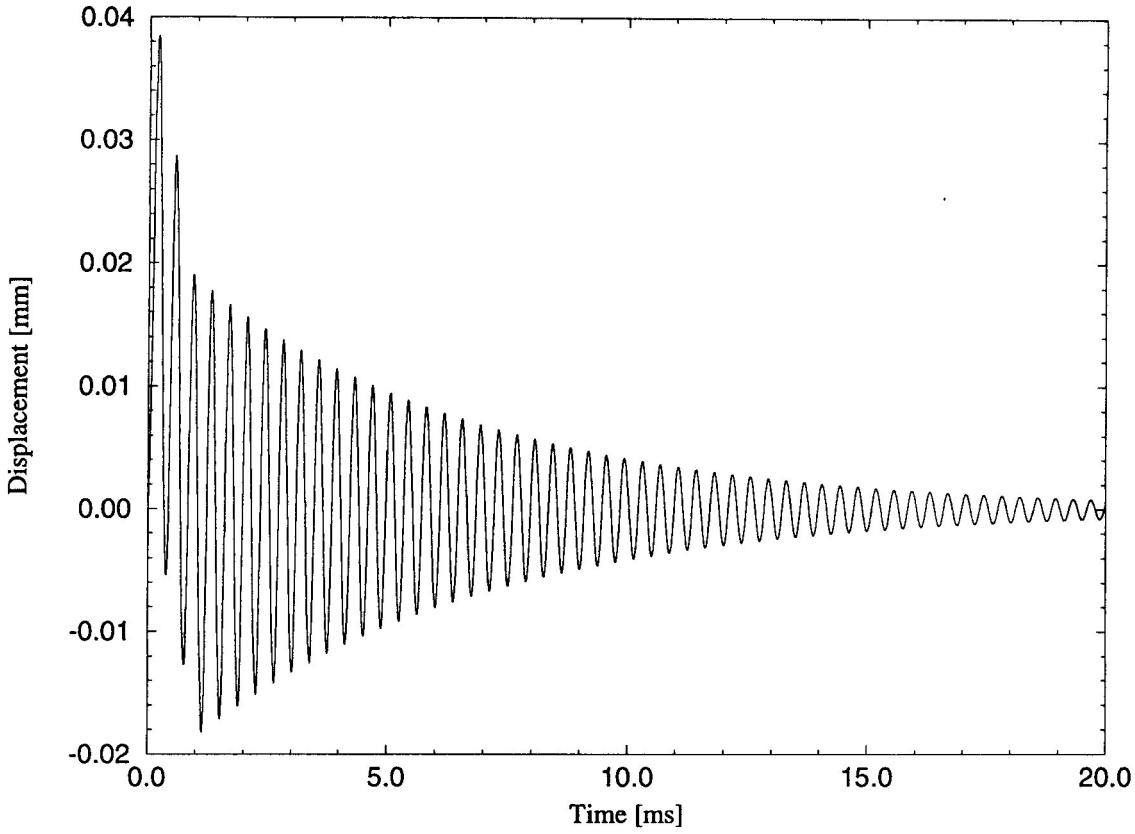

Fig. 6.2. Radial displacement of the NIF minichamber shell.

The maximum stress in the spherical shell (7.7 MPa) is well below the yield strength of 6061 aluminum (270 MPa at room temperature). In the above analysis, none of the typical stress risers, such as perforations in the shell and boundary conditions, were modeled. In an actual structure the maximum stress could be as much as an order of magnitude larger. Also, the possibility of brittle fracture or fatigue fracture at the low operating temperature has not yet been addressed.

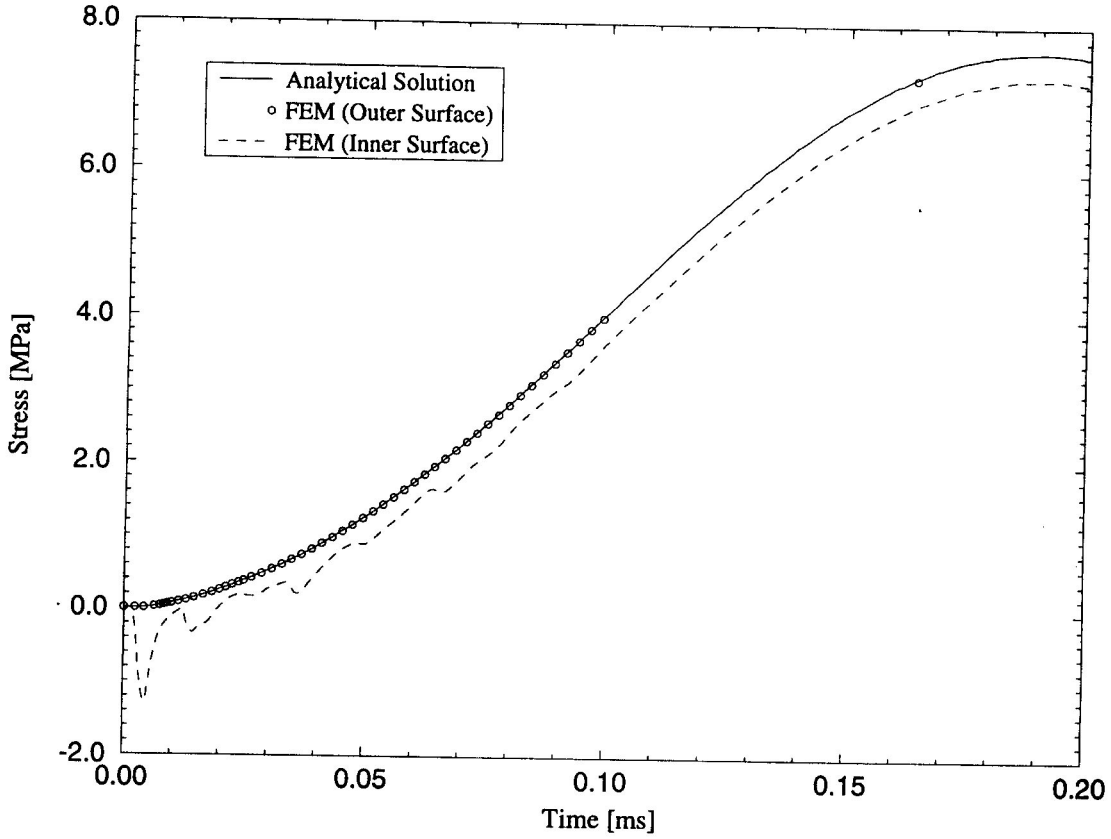

Fig. 6.3. In-plane membrane stress of the NIF minichamber shell.

6.5 References

[6.1] *Energy and Technology Review - The National Ignition Facility*, Lawrence Livermore National Laboratory, Livermore, CA, December 1994.

[6.2] *National Ignition Facility Conceptual Design Document*, L-16973-1, Lawrence Livermore National Laboratory, Livermore, CA.

[6.3] J. Gere and S. Timoshenko, "Mechanics of Materials," PWS Engineering, Boston, MA, 1984.

[6.4] F. R. Schwartzeber et al. (eds.), "Cryogenic Materials Data Handbook," *Tech. Documentary Dept*. ML-TDR-280, Clearinghouse for Federal Scientific and Technical Information, Springfield, VA, 1965.

[6.5] W. Soedel, "Vibrations of Shells and Plates," Marcel Dekker, New York, NY, 1993.

7. CHAMBER CHARACTERISTICS/RECOMMENDATIONS

7.1 General Perspectives

Each of the chamber scoping studies summarized in the previous sections dealt with investigations of the dynamic response of either a spherical or cylindrical shell subjected to severe blast loadings. The basic critical issues involving the design of the target chamber were common to each, i.e., the chambers needed to contain the intense mechanical and thermal loading for single or multiple shots over a specified lifetime. For most cases, the mechanical and thermal responses were decoupled by employing the use of thermal liners on the first wall surface. Consequently, the studies reported here primarily focused on the mechanical analysis of the shell structure.

The first observation to be made on the choice of target chamber geometry is the fact that a spherical structure is the optimum shape to contain a uniform, spherically symmetric pressure load emanating from a target explosion. However, due to more practical manufacturing and maintenance considerations, as well as the need for diagnostic access, a cylindrical chamber was often chosen instead. When afterpressures (or residual pressures) of significant magnitude were components of the pressure loading, the requirement for extra volume necessitated the use of cylindrical vessels with easily attached end caps.

For the mechanical analysis of either cylindrical or spherical shells, the classic equations of motion yield the response which can be used for a scoping study if the shells are not highly perforated. That is, the dynamic response of the shell can be simulated by numerically integrating the differential equations of motion using the pressure history as a forced excitation or impulsive loading. As a general rule, if the duration of the pressure pulse is less than one tenth the fundamental period of vibration of the shell, the loading can be considered impulsive [7.1]. The characteristic response of the shell in this case is free vibration with an initial velocity. Using modal superposition methods for the shell results in displacement and stress histories that correspond to the superposition of all modes of the shell that are initially excited. For example, with the symmetry involved in the dynamic loading of a spherical shell with a uniform, radial pressure pulse, only the first extensional breathing mode of the spherical vessel will contribute to the response [7.2]. In this case, the maximum stress will correspond to the in-plane membrane (extensional) response. On the other hand, with a cylindrical shell, the total response may be a combination of the breathing mode with higher frequency flexural modes superimposed. End conditions, or support conditions, are important considerations in this case [7.3, 7.4]. The vibrational modes that are excited depend on whether or not the cylindrical shell is allowed to expand or contract axially. For a cylindrical shell that is clamped (or completely constrained) on the ends, the

location of the maximum stress is at these rigid supports. However, localized stresses can be reduced by increasing the wall thickness in this region.

If a shell structure is highly perforated, the shell becomes more compliant and no longer displays the characteristic response of a continuous system. Vibrational modes are much more complex and more difficult to predict. Usually the maximum stresses are in the ligaments if the perforations are effectively reinforced. Recently, proposed chamber designs (such as NIF) have such a large percentage of wall surface used for ports, that the only effective method of analysis is finite elements (FE). For example, we have now developed full three dimensional (3-D) finite element models of cylindrical shells that allow for circular or elliptical perforations arranged in rows and columns in either a square or triangular pattern. The perforations may also have reinforcement around the edges. For spherical geometries we have both axisymmetric or full 3-D models. Figure 6.3 illustrated how the stresses obtained from our FE model of the spherical NIF minichamber matched our previous analytical solutions. Current modeling efforts include integrating the solid modeling or CAD files with the finite element software. For example, ProEngineer is being used in conjunction with the finite element software ANSYS to automatically create the mesh and perform static and transient analyses on shell structures.

Finally, for investigations involving fatigue calculations, it was important to include the shell stresses that might arise due to residual afterpressures. When computing transient and steady-state wall responses, the gradual rise in overpressure often resulted in rather large mean stresses. This had to be included in the fatigue study, since mean stresses could drastically reduce fatigue life.

ACKNOWLEDGEMENT

Support for this work was provided by Forschungszentrum Karlsruhe, through Fusion Power Associates.

7.2 References

[7.1] J. Biggs, "Structural Dynamics," McGraw Hill, Inc., New York, NY, 1964.

[7.2] W. Soedel, "Vibrations of Shells and Plates," Marcel Dekker, New York, NY, 1993.

[7.3] J. Powers, "Structural and Fatigue Analysis of the Sandia Laboratory Microfusion Reactor Chamber," M.S. Thesis, Mechanical Engineering Department, University of Wisconsin - Madison, 1991.

[7.4] D. Adler, "The Effect of End Conditions on the Axisymmetric Vibrations of Cylindrical Shells," M.S. Thesis, Mechanical Engineering Department, University of Wisconsin - Madison, 1993.